Resource

Cell Reports

High-Dimensional Phenotyping Identifies Age-Emergent Cells in Human Mammary Epithelia

Graphical Abstract

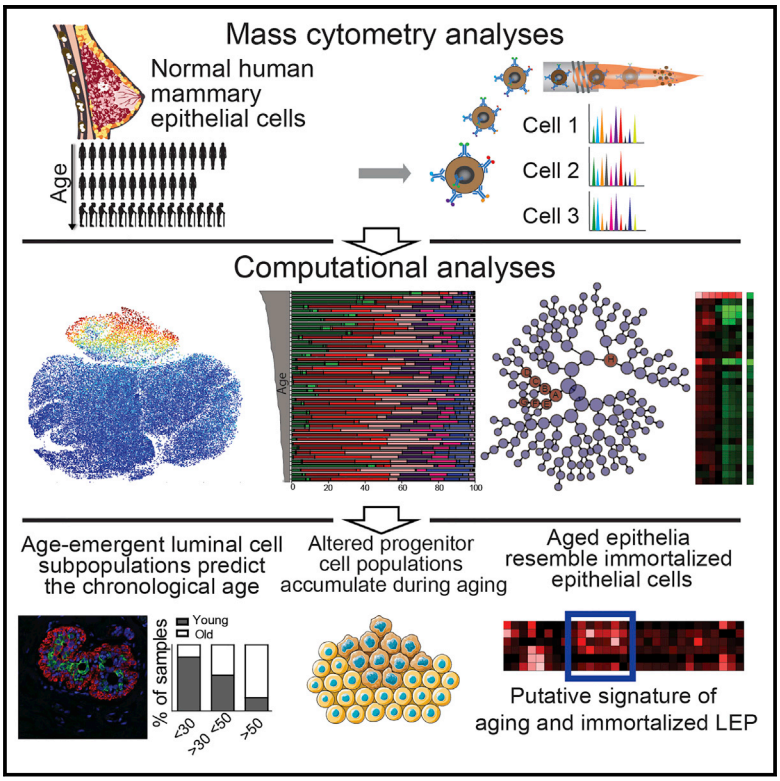

Authors

Fanny A. Pelissier Vatter, Denis Schapiro, Hang Chang, ..., Mark A. LaBarge, Bernd Bodenmiller, James B. Lorens

Correspondence

mlabarge@coh.org (M.A.L.), bernd.bodenmiller@imls.uzh.ch (B.B.), jim.lorens@uib.no (J.B.L.)

In Brief

Vatter et al. find that single-cell mass cytometry of human mammary epithelial cells from 57 women, from 16 to 91 years old, depicts an in-depth phenotyping of aging mammary epithelia. Subpopulations of altered luminal and progenitor cells that accumulate with age may be at increased risk for oncogenic transformation.

Highlights

- CyTOF analysis reveals human mammary epithelial heterogeneity with age
- Age-emergent luminal cells share phenotypes with candidate breast cancer cells of origin
- Classification models correctly assign tissue samples to their age group
- Age-related changes are conserved between mammary epithelial tissue and primary cells

Pelissier Vatter et al., 2018, Cell Reports *23*, 1205–1219
April 24, 2018
https://doi.org/10.1016/j.celrep.2018.03.114

CellPress

Cell Reports
Resource

High-Dimensional Phenotyping Identifies Age-Emergent Cells in Human Mammary Epithelia

Fanny A. Pelissier Vatter,[1,2] Denis Schapiro,[3] Hang Chang,[4] Alexander D. Borowsky,[5] Jonathan K. Lee,[4] Bahram Parvin,[6] Martha R. Stampfer,[3] Mark A. LaBarge,[2,4,7,8,*] Bernd Bodenmiller,[3,8,*] and James B. Lorens[1,2,8,9,*]

[1]Department of Biomedicine, University of Bergen, Bergen 5009, Norway
[2]Centre for Cancer Biomarkers (CCBIO), University of Bergen, Bergen 5009, Norway
[3]Institute of Molecular Life Sciences, University of Zürich, 8057 Zürich, Switzerland
[4]Biological Systems and Engineering Division, Lawrence Berkeley National Laboratory, Berkeley, CA, USA
[5]Department of Pathology and Laboratory Medicine, Center for Comparative Medicine, University of California, Davis, School of Medicine, Sacramento, CA, USA
[6]Department of Electrical and Biomedical Engineering, University of Nevada, Reno, NV, USA
[7]Department of Population Sciences & Center for Cancer and Aging, City of Hope, Duarte, CA, USA
[8]These authors contributed equally
[9]Lead Contact
*Correspondence: mlabarge@coh.org (M.A.L.), bernd.bodenmiller@imls.uzh.ch (B.B.), jim.lorens@uib.no (J.B.L.)
https://doi.org/10.1016/j.celrep.2018.03.114

SUMMARY

Aging is associated with tissue-level changes in cellular composition that are correlated with increased susceptibility to disease. Aging human mammary tissue shows skewed progenitor cell potency, resulting in diminished tumor-suppressive cell types and the accumulation of defective epithelial progenitors. Quantitative characterization of these age-emergent human cell subpopulations is lacking, impeding our understanding of the relationship between age and cancer susceptibility. We conducted single-cell resolution proteomic phenotyping of healthy breast epithelia from 57 women, aged 16–91 years, using mass cytometry. Remarkable heterogeneity was quantified within the two mammary epithelial lineages. Population partitioning identified a subset of aberrant basal-like luminal cells that accumulate with age and originate from age-altered progenitors. Quantification of age-emergent phenotypes enabled robust classification of breast tissues by age in healthy women. This high-resolution mapping highlighted specific epithelial subpopulations that change with age in a manner consistent with increased susceptibility to breast cancer.

INTRODUCTION

Adult tissue stem and progenitor epithelial cells generate differentiated daughter cells for tissue remodeling and homeostasis (Biteau et al., 2008; Mansilla et al., 2011). Evidence suggests skewed stem cell function contributes to diseases of aging (Sharpless and DePinho, 2007). Human breast epithelium, comprised of apical luminal epithelium (LEP) and basal myoepithelium (MEP) cell layers surrounded by a basement membrane, undergoes remarkable growth and remodeling between puberty and menopause and during lactation, supported by stem and progenitor cells. The greatest risk factor for breast cancer is age and exclusively genetic explanations are inadequate (LaBarge et al., 2016; Stephens et al., 2012). Differentiation-defective progenitor cells accumulate and tumor-suppressive MEPs decline with age, while older LEPs display basal properties, such as nuclear-localized YAP and MEP gene expression (Chen et al., 2014; Garbe et al., 2012; Pelissier et al., 2014; Skibinski et al., 2014). We hypothesize that these age-associated changes elevate cancer risk. Congruently, LEPs from women with high cancer risk (e.g., BRCA1/2 carriers) show basal characteristics, and luminal progenitors with a basal phenotype are suggested cells of origin for murine mammary adenocarcinoma (Lim et al., 2009; Molyneux et al., 2010; Proia et al., 2011). We therefore sought to gain insight into molecular changes in the mammary epithelium during aging and comprehensively catalog age-emergent phenotypic diversity using mass cytometry (Bandura et al., 2009) in samples from women aged 16–91 years old.

RESULTS

High-Dimensional Analysis of Cellular Heterogeneity within Human Mammary Epithelia

To measure age-emergent phenotypic diversity in the human breast, we used mass cytometry to obtain single-cell proteomic profiles of cryopreserved normal primary human mammary epithelial cell (HMEC) strains at passage four, from 44 women of ages 16 to 91 years old (Figure 1; Table S1). A 29-antibody panel recognizing human mammary epithelial lineage markers and intracellular signaling proteins was used to establish high-dimensional phenotypes of single HMECs (Figure S1; Table S2) (dos Santos et al., 2013; LaBarge et al., 2007; Lim et al., 2009; Regan et al., 2012; Taylor-Papadimitriou et al., 1989; Villadsen et al., 2007). Simultaneous analysis of $\geq$20,000 HMECs from each of the women from three age groups (<30 years, n = 16; >30 years < 50 years, n = 13; and >50 years, n = 15) measured 29 protein epitope dimensions (Ds) (Figure 1A). Non-linear dimensionality reduction, t-distributed stochastic neighbor

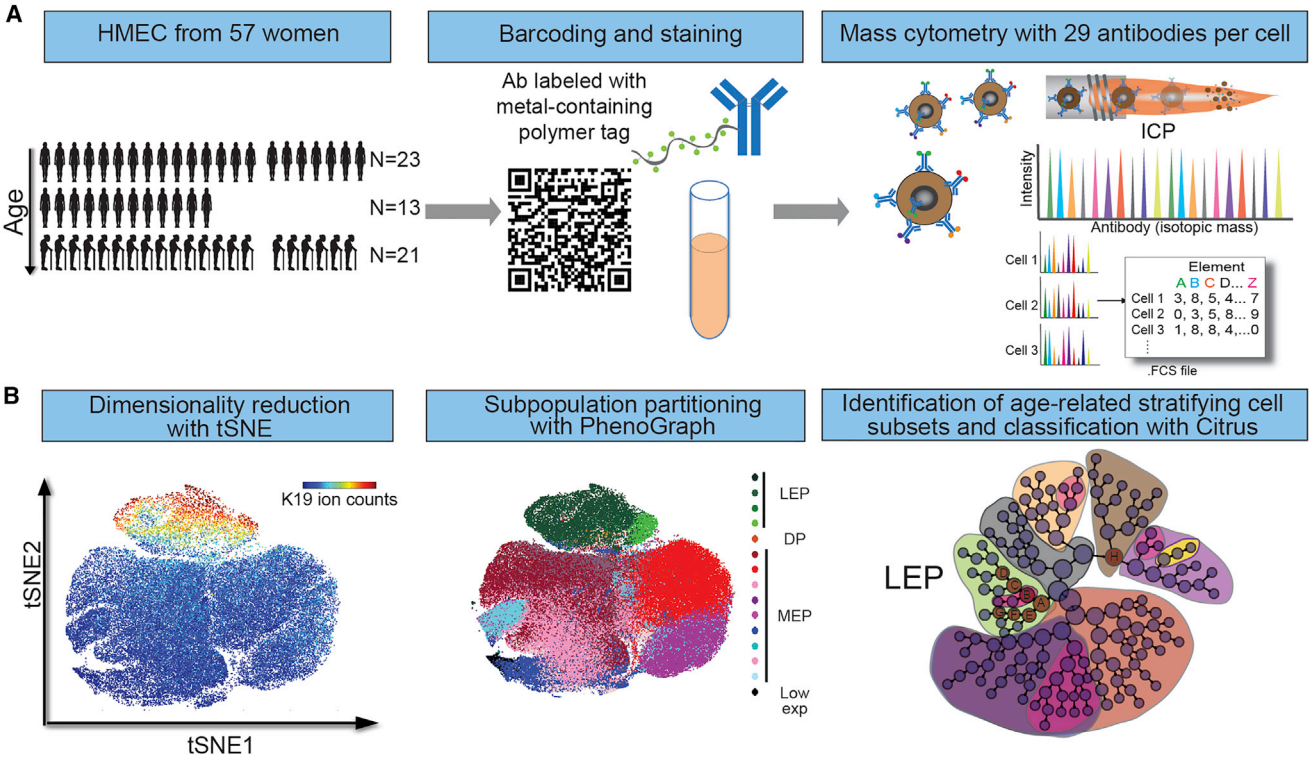

Figure 1. Mass Cytometry Analysis of Human Mammary Epithelial Cells

(A) Summary of experimental design. 57 samples of HMECs from women aged 16 to 91 years old (comprising 13 uncultured breast epithelia samples and 44 primary cultured HMEC strains at passage 4 [p4]) were barcoded and stained using a panel of 29 antibodies labeled with isotope tags and analyzed using mass cytometry.

(B) Strategy to analyze high-dimensional single-cell data and identify lineage and age-related phenotypic divergence.

See also Tables S1 and S2 and Figure S1.

embedding (tSNE) (Amir et al., 2013), created a 2D map of the entire dataset at single-cell resolution with similar phenotypes proximal to each other (Figure 1B). Distinct LEP (K19+/K7+/K8/18+/CD133+) and MEP (K14+/K5/6+) cell populations were distinguishable on the tSNE map (Figure 2A). Several signaling markers showed lineage dependence, especially in MEPs; CD44, YAP, phospho-epidermal growth factor receptor (pEGFR), pStat1, pS6, and p-Phospholipase C Gamma 2 (pPLCγ2), previously implicated in myoepithelial function and contractility (Pasic et al., 2011), were prevalent in the MEP cell population (Figures 2A, S1B, and S1C). The partial superposition of K14+ and K5/6+ cell population revealed the high degree of heterogeneity. A small subpopulation of cells with low marker expression also was noted, which may have corresponded to the K14−/K19− epithelia previously described (Villadsen et al., 2007), and it was not further examined.

To address how aging affects the human mammary epithelium, we first demarcated LEP and MEP populations using a manual K19 gate (Figure 2A). K19, K7, K8/18, CD133, and cKit expression was high in LEPs, while K14 and K5/6 expression was higher in MEPs (Figure 2B). LEPs exhibited higher phospho-nuclear factor κB (pNF-κB), which is implicated in mouse mammary epithelial proliferation and branching (Brantley et al., 2001). MEPs had increased expression of basal markers (Axl, pS6, pPLGγ2, pEGFR, CD44, pGsk3, and pStat1) involved in myoepithelial homeostasis (Pasic et al., 2011). The phenotypic space projections on the tSNE maps were similar among the three age groups (Figure 2A), however, the expression levels of a number of markers changed significantly with age (Figures S2 and S3). The most prominent age-related difference was observed in the LEP population, where K14 and YAP expression increased and K19 and K7 decreased with age (Figures 2C and S3B). Overall these results revealed remarkable phenotypic heterogeneity within the mammary epithelia.

Intra-lineage and Age-Related Phenotypic Divergence in HMECs

The tSNE map displayed regions of cell density (Figure 2A) and K14, K5/6, pRb, and CyclinB1 expression within the MEP lineage, indicative of distinct cellular subpopulations (Figures 2A and S1C). Intra-lineage subpopulations were identified as distinct clusters of cells with shared phenotypes using PhenoGraph (Levine et al., 2015) (Figures 3A and S4A). There were four LEP (LEP1–LEP4) and nine MEP (MEP1–MEP9) clusters (Figure 3B). One subpopulation, denoted double positive (DP, between 120 and 503 non-doublet cells), co-expressed K14 and K19 in a separate phenotypic space between the LEP and MEP populations. This DP population likely comprised epithelial

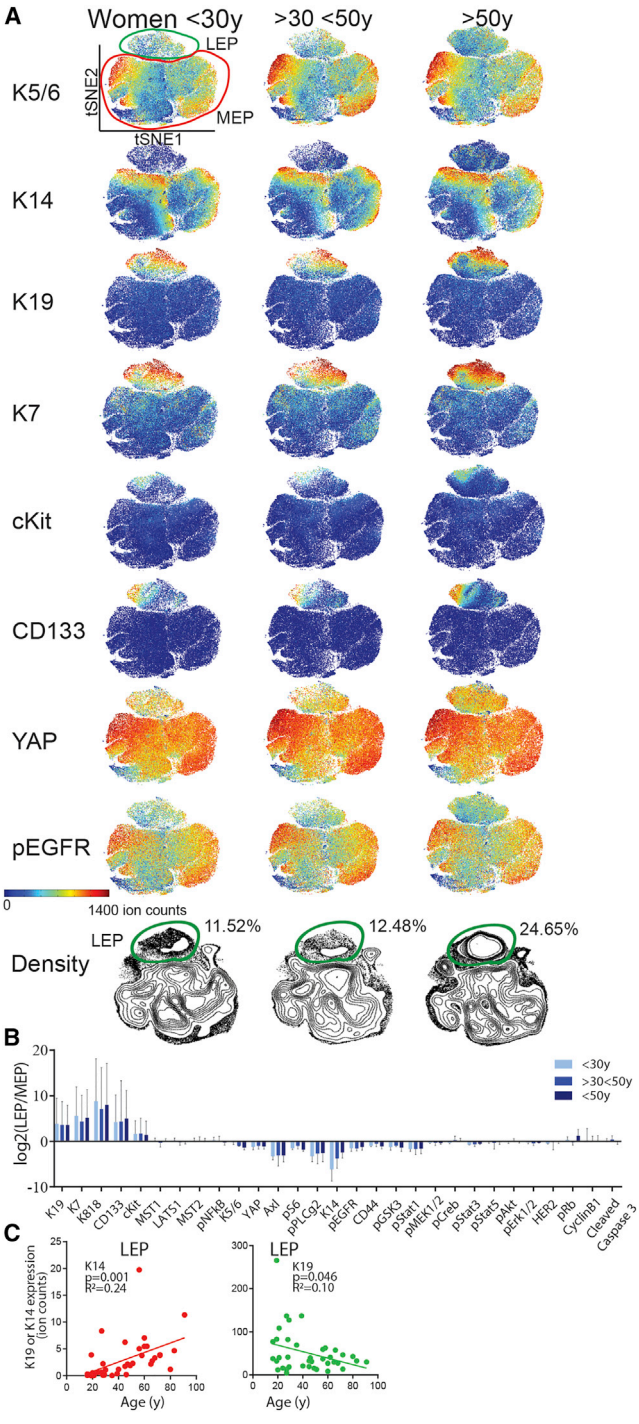

Figure 2. Collective tSNE Analysis Distinguishes Major Luminal and Myoepithelial Lineages

(A) The raw data have been transformed with arcsinh with the cofactor of 5. tSNE maps from HMECs at p4 from women <30 years old (merged and subsampled at 50,000 cells, n = 16), >30 < 50 years old (n = 13), and >50 years old (n = 15).

(B) Log_2 fold change of marker expression of LEP over MEP manually gated from tSNE projection map in HMECs from women <30 years old, >30 < 50 years old, and >50 years old. Data are log_2 of ratio of median ± SD.

progenitors (Villadsen et al., 2007). A small subpopulation of cells with low marker expression was not further examined (<0.52 ion counts per cell). The LEP3 cluster showed high levels of pRb and CyclinB1, indicative of higher proliferation compared to the other LEP subpopulations (reviewed in Giacinti and Giordano, 2006). Clusters MEP4 and MEP7 expressed higher levels of CyclinB1 that correlated with higher DNA content (iridium intercalator counts; Figure S4B) compared to the other MEP subpopulations.

Age-related changes in marker expression were observed mainly within the LEP subpopulations. Heatmaps of marker expression in each PhenoGraph cluster, in HMECs from women >30 and <50 years old (Figure 3C) and women >50 years old (Figure 3D), were normalized to values from <30-year-old women to highlight age-related changes. Increased K14 and decreased K19 expression was observed with age in LEP2, LEP3, and LEP4 clusters from women >30 and <50 years old and in all LEP subpopulations from women >50 years old. In addition to phenotypic changes with age, the abundance of the LEP clusters significantly increased, whereas abundance of MEP2, MEP5, and MEP8 clusters significantly decreased with age (Figure 3E). This trend was observed at the individual level, with high inter-sample heterogeneity (Figure 3F). We previously reported age-related changes in LEP and MEP cells *in vivo* based on K14/K19 staining, and 4 lineage markers (Garbe et al., 2012) did not discern the degree of heterogeneity apparent in this new analysis. Prominent changes in marker expression and abundance occurred in three of four LEP types as early as middle age, and all four types change beyond 50 years. Indeed, the abundance of LEP1 increased more than 3-fold. Decreased abundance of MEP also was type specific.

Correspondence analysis (CA) provided a global understanding of the relationships between all PhenoGraph clusters and the age factor (Härdle and Simar, 2007). CA reduces high-dimensional observations to a smaller set of explanatory components, allowing visualization of data on each woman and PhenoGraph subsets in the same space (Figure 3G). Women >50 years old were associated with LEP1–4 subsets and women <30 years old were associated with MEP1–9 subsets, probably reflecting the relative abundance of those lineages with age. The DP subset, which represents progenitor cells, was associated mainly with older women. The first component, contributing 43.2% and comprising mainly LEP1, captured the tendency of older women to have more LEP (Figures 3G and 3H). The second component (27.5%) provided a different ordering. Altogether, there was a significant association between an age-dependent luminal subset and the chronological age of the primary epithelial cells.

Unsupervised agglomerative hierarchical clustering (Citrus) was used to examine age-dependent changes in an orthogonal manner. Multidimensional single-cell data were distilled to a hierarchy of marker expression-related clusters, and cluster-specific cell frequency changes were determined (Bruggner et al., 2014). Seven clusters were identified (Figures 4A–4C) that were significantly more abundant with age (prediction error of 26% as

(C) K19 and K14 expression in LEP as a function of age. 250MK, 90P, 245AT, 173T, and an outlier 42P were excluded from the analysis.

See also Figures S1–S3.

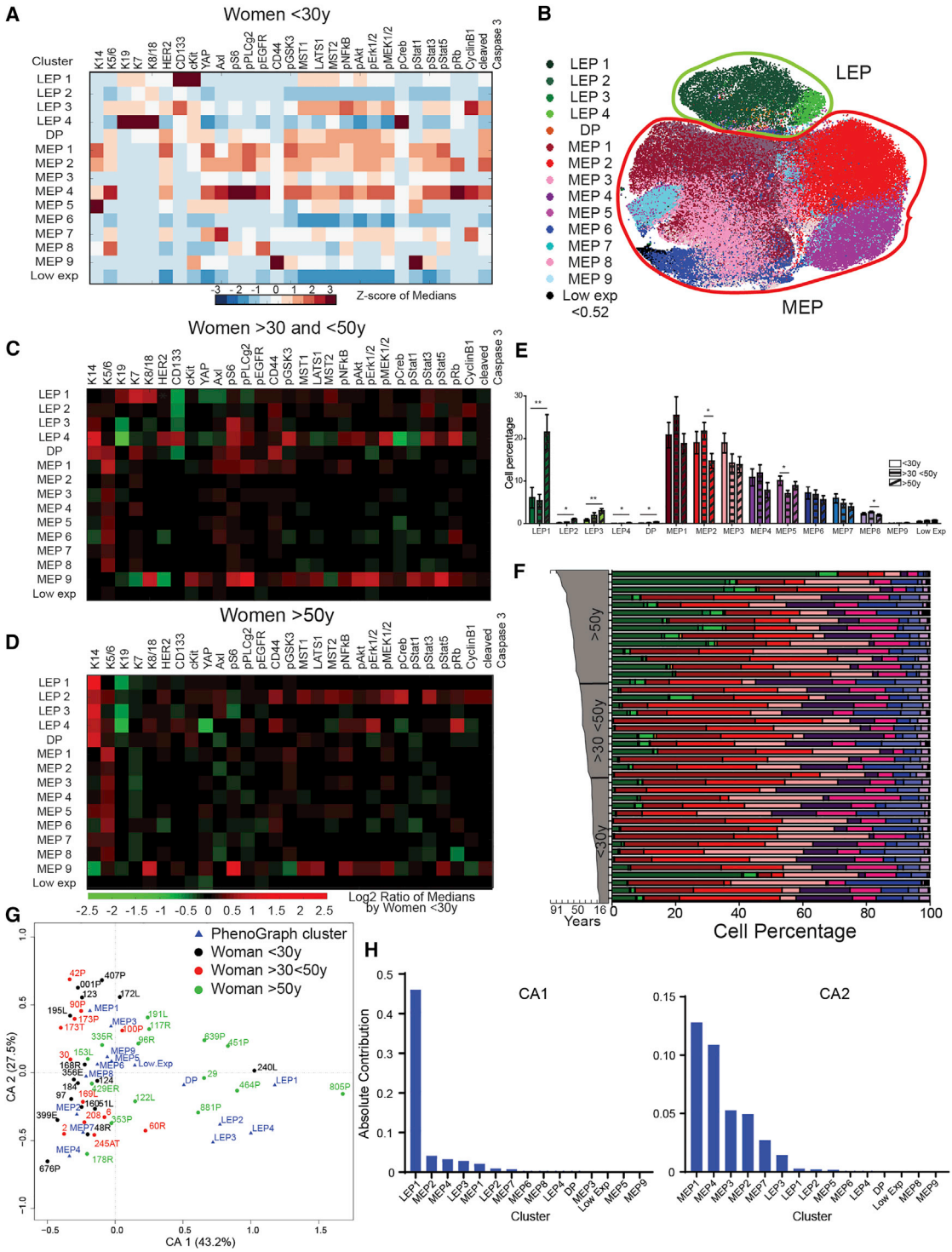

Figure 3. Age-Related Phenotypic Divergence in the Landscape of HMECs

(A) Heatmaps of marker expression in PhenoGraph clusters of HMECs from women <30 years old (*Z* score scale, merged, n = 16) (excluding 250MK, 90P and 245AT, 173T).

(B) tSNE projection of the PhenoGraph clusters identified with PhenoGraph identified in (A), colored by cluster.

(C and D) Heatmaps of marker expression in each PhenoGraph cluster in HMECs from (C) women >30 and <50 years old and (D) women >50 years old, normalized to values from <30-year-old women.

(E) Plots of cell percentage in each PhenoGraph cluster (excluding 250MK, 90P and 245AT, 173T). Data are mean ± SEM.

(legend continued on next page)

estimated by cross-validation and a p value < 0.05 using a Student's t test) (Figure 4A; Figure S4D), all of which represented the LEP compartment. Figure S4C illustrates the agglomerative clustering. The LEP subpopulations that showed age-dependent changes had specific marker expression signatures consistent with acquired MEP/basal-like characteristics (Figures 4A and 4B; Figure S4G). The age-emergent LEP clusters were all higher in K14 compared with the <30-year LEP. Cluster A, residing at the apex of the hierarchy, was $K19^{low}$ and $K14^{high}$ (Figures S4E and S4G). Clusters B, C, and D showed higher YAP, HER2, cKit, Axl, pS6, pPLCγ2, pEGFR, CD44, pGSK3, pNF-κB, pAkt, pERK1/2, pMEK1/2, pStat1, pStat3, and pStat5 expression than <30-year LEP. Most of these markers are associated with proliferation and migration and are mainly expressed in young MEP. Each cluster had defining characteristics, e.g., cluster B had the highest pRb and CyclinB1 expression that correlated with higher DNA content (Figure 4B; Figure S4F). Only cluster H decreased in abundance with age (Figures 4A, 4C, and S4D), and it mapped to the MEP compartment of the tSNE landscape. Those cells expressed low levels of K14, pS6, CyclinB1, and pRb (Figure S4F), possibly indicative of a quiescent, terminally differentiated MEP.

Collectively, these results indicated that a subset of LEP acquires a basal phenotype and accumulates while a subset of MEP decreases in abundance with age.

Age-Emergent Epithelial Cells in Primary Breast Epithelia

To confirm our findings, we conducted mass cytometry profiling using the 29-antibody panel on epithelial cells ($\geq$10,000 cells per sample) derived from uncultured breast epithelia samples obtained from 13 women of different ages (<30 years, n = 7 and >50 years, n = 6; Table S1). As predicted by the HMEC analysis, the tSNE map revealed extensive phenotypic heterogeneity in the breast epithelia (Figure 5A; Figure S5A). Unsupervised clustering identified four distinct phenotypes of LEP (LEP1–4), seven types of MEP (MEP1–7), a DP subpopulation (between 13 and 719 non-doublet cells), and a low-expressing cell phenotype (<18.32 ion counts per cell) (Figure 5B). Protein expression patterns were consistent with these phenotypic designations and with the HMEC analysis (Figure 5C). K19, K7, K8/18, CD133, and cKit expression was high in LEP, while MEP showed higher expression of basal markers (K14, K5/6, Axl, pS6, CD44, pEGFR, and pStat1). The abundance of the LEP1 subpopulation significantly increased, whereas the abundance of MEP2 significantly decreased with age (Figure 5D), a trend also observed at the individual level (Figure 5E). Citrus analysis identified three clusters that were significantly more abundant with age (Figure 5F; Figure S5B), all residing within the LEP compartment of the tSNE phenotypic landscape. All three LEP clusters (A, B, and C) showed age-dependent changes in specific marker expression signatures, consistent with acquired MEP/basal-like characteristics (Figure 5G; Figure S5C). To quantify the extent of acquired MEP-like/basal phenotype, we calculated the geometric distance between the breast epithelia or HMEC LEP Citrus clusters and their respective MEP populations. This demonstrated that the LEP-MEP phenotypic distance was reduced by 26.7% and 32% in the breast epithelia and HMECs with age, respectively (Figure 5H). Collectively, this finding supports the notion that age-emergent epithelial cells derived from uncultured breast epithelia samples showed phenotypes that matched those identified in the primary cultured HMECs.

Age-Emergent Phenotypes Predict Breast Tissue Age *In Vivo*

As the $K14^{high}K19^{low}$ clusters from both breast tissue and HMECs formed the apex of the age-dependent cluster hierarchy, we hypothesized that the expression pattern of these cytokeratins could be used to predict the approximate age of normal breast tissue. Human breast sections were stained with anti-K14 and anti-K19 (<30 years, n = 52 [10 women]; >30 < 50 years, n = 86 [25 women]; and >50 years, n = 33 [15 women]) (Figure 5I), and a classification model was built using morphometric context (Chang et al., 2013). At least 1,000 cells per section were analyzed. This computational approach relied on automated cell segmentation, with manual curation, to define different epithelial cells prior to quantification of single-cell K14 and K19 levels and morphometric features. The machine learning-based classification model correctly assigned more than 50% of the samples into their correct age group, as compared with a random guess of 33.3% (Figure 5J), based on the higher level of K14 and lower level of K19 in LEP with age, as observed on the tissue sections (Figure 5I). These data validated predictions from the mass cytometry data, and the *in situ* analysis demonstrated quantifiable age-related changes in LEP in breast tissue.

Next, we used age-dependent phenotypic divergence to build a second classification model to test the hypothesis that age-related changes in marker expression from our statistical analysis would generalize to an independent dataset. This second model was based on the totality of the mass cytometry data, and it was not restricted to K14 and K19. In general, classification models use cross-validation to avoid testing hypotheses suggested by the data (type III errors). Using a training set of 5 HMECs each from women in the <30-year and >50-year age groups, we successfully assigned 13/16 women <30 years old and 12/15 women >50 years old (Figure 5K). The classification performance was increased with the number of training samples (Figure S6A). Strikingly, the HMEC strains that were incorrectly

(F) Intra-sample heterogeneity for each woman is represented graphically by a horizontal bar in which segment lengths represent the proportion of the sample assigned to each cluster, colored accordingly (excluding 250MK).
(G) The first two components of correspondence analysis (CA), accounting for 70% of the co-association structure between PhenoGraph subpopulations and different strains. Proximity among women and among clusters indicates similarity, however, only a small angle connecting a woman and a cluster to the origin indicates an association. The angle between women <50 years old and LEP was statistically smaller than the angle between women <30 years old and women >30 and <50 years old and LEP (t test, p < 0.001). PhenoGraph subsets are displayed as triangles and HMEC samples as circles.
(H) Contributions of the PhenoGraph subpopulations to CA-1 and CA-2.
See also Figure S4.

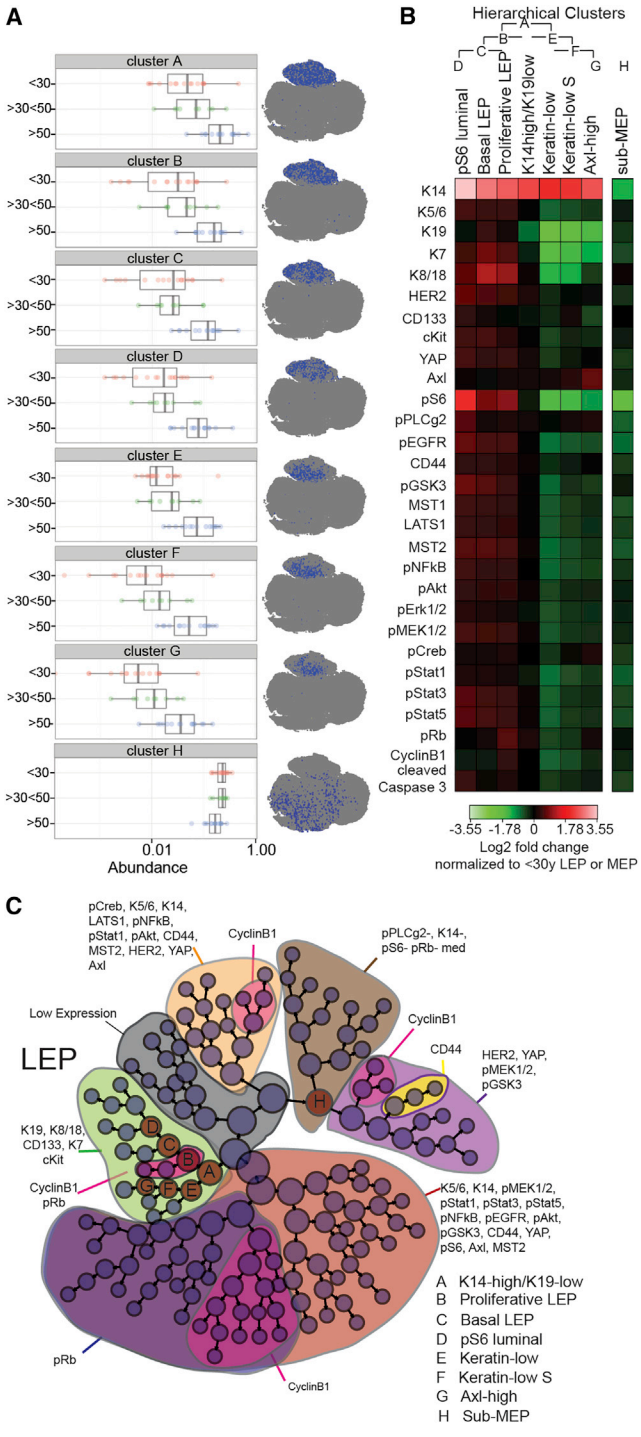

Figure 4. Evidence of Age-Dependent Phenotypic Divergence in the Luminal Population

The Citrus algorithm was applied to identify cell populations by hierarchical clustering of phenotypically similar cells from an aggregate dataset from all samples (excluding 250MK, 90P and 245AT, 173T). A defining characteristic of each cluster is denoted as follows: cluster A, K14^{high}/K19^{low}; cluster B, proliferative LEP; cluster C, basal LEP; cluster D, pS6 luminal; cluster E, Keratin^{low}; cluster F, Keratin-low S; cluster G, Axl^{high}; and cluster H, sub-MEP.

(A) Boxplots of cell abundance in each age-related cluster and its representative tSNE phenotypic projection. Each data point on these graphs represents the proportion of the cluster cell number compared to the total cell number in a single sample. The log10 scale represents an abundance of cells from 0 to 1.

(B) Heatmaps of marker expression of each cluster normalized to LEP from <30-year-old women for clusters A to G and MEP from <30-year-old women for cluster H.

(C) Hierarchical tree of agglomerative clusters obtained with the Citrus analysis. Node sizes are scaled on the basis of frequency of cells in each cluster. See also Figure S4.

classified as "old" were derived from tissue peripheral to a breast tumor, harbored a known high cancer risk mutation, or had LEP proportions above the mean, while a >50-year HMEC strain with decreased LEP proportion was incorrectly assigned as "young." Hence, the classification model validated the hypothesis that subsets of luminal cells change with age and can be used as age predictors, and it suggested that this information could be a relevant indicator for cancer risk.

Age-Emergent Luminal Cells Acquire Increased Basal Function

Next we investigated the functional consequences associated with the age-related basal phenotypic changes in the mammary luminal compartment. MEPs form cell-cell contacts with both LEPs and other MEPs and adhere to the basement membrane (Bergstraesser et al., 1995; Pitelka et al., 1973). These adhesive properties are characteristic of MEP, whereas LEP-extracellular matrix interactions are relatively minimal (Cerchiari et al., 2015). We hypothesized that the increased basalness of older LEPs would affect their cell adhesion and migratory capacity. Cell migration kinetics was measured by real-time impedance in LEP and MEP cells, sorted via fluorescence-activated cell sorting (FACS), from 6 different primary HMEC strains. LEPs isolated from women <30 years old migrated faster than isogenic MEPs (Figures S6B and S6C). In contrast, LEPs from women >50 years old migrated much slower and at a rate comparable to the cognate MEPs (Figures S6B and S6C), consistent with increased basal adhesion properties.

In addition, EGFR-mitogen-activated protein kinase (MAPK) pathway activation (pEGFR, pMEK, pErk, and pAkt) was higher in MEPs than in LEPs (Figure 2A; Figure S1), and it was higher in the LEP clusters that changed in abundance with age (Figure 4B). Therefore, we evaluated age-dependent differences in HMEC responses to EGF. HMECs from 3 women <30 years old and 3 women >50 years old were treated with EGF combined with vanadate, and signal transduction was measured by mass cytometry (Figures S6D–S6F). Both LEPs and MEPs exhibited EGFR pathway activation within the time course (Figure S1B); however, pStat, pEGFR, pErk, pMEK, and pPLCγ2 levels were increased in LEPs from women >50 years old compared to younger women. tSNE analysis revealed a subpopulation of HMECs with activated EGFR (Figure S6E). LEPs derived from older women were more prevalent in this population, consistent with increased EGF-signaling capacity (Figure S6F). Thus, older LEPs acquired myoepithelial-like adhesion and migration characteristics, as well as an increased EGF signaling.

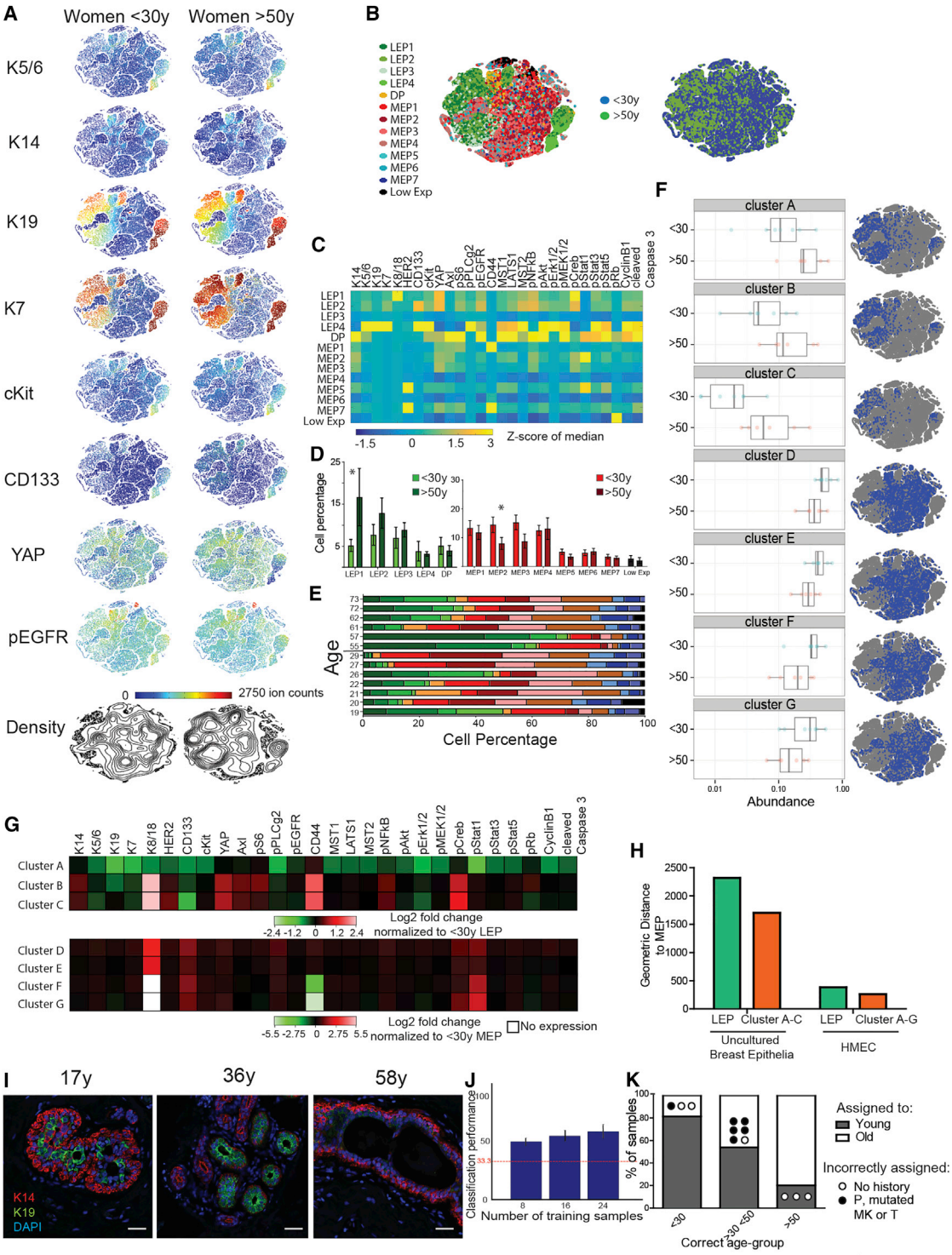

Figure 5. Age-Related Phenotypic Divergence in Uncultured Breast Epithelia

(A) tSNE maps from dissociated uncultured breast epithelia from women <30 years old (merged and subsampled at 50,000 cells, n = 7) and >50 years old (merged and subsampled at 50,000 cells, n = 6). The pGsk3 channel was removed from the analysis due to a technical issue.

(B) tSNE projection of the PhenoGraph clusters. The tSNE projection (right panel) of women <30 years old (blue) and women >50 years old (green) is shown.

(C) Heatmaps of *Z* score of marker expression in PhenoGraph clusters of uncultured breast epithelia from women <30 years old (merged, n = 7).

(D) Plots of cell percentage in each PhenoGraph cluster. Data are mean ± SEM.

(legend continued on next page)

Age-Dependent Phenotypic Divergence in the Luminal Progenitor Population

We next asked whether the prominent age-related changes in LEPs were the result of changes in luminal progenitors (LPs). Luminal-biased progenitors expressing cKit (Lim et al., 2009) were FACS enriched from HMEC strains derived from 3 women <30 years old and 3 women >50 years old at passage 4, and they were analyzed by mass cytometry using 12 mammary epithelial progenitor and lineage markers (Figure 6A). Unsupervised agglomerative clustering identified two LP clusters that were more abundant (A and B) and one cluster that was less abundant (C) with age (Figure 6B; Figure S7A). These clusters localized within the luminal compartment of the tSNE phenotypic space, and they displayed specific marker signatures (Figure 6C; Figure S7D): cluster A was $K7^{high}$ while cluster B was $K19^{high}$. Both of these clusters displayed high expression of CD133, cKit, HER2, and YAP, establishing an age-emergent LP marker signature; thus, cKit+/CD133− and cKit+/CD133+ LP cells were FACS enriched from HMECs at passage 4. A higher proportion of cKit+/CD133+ LPs were present in older women (Figure 6D). The older cKit+/CD133+ LPs generated more acini in a Matrigel/collagen 3D embedding assay (Figure 6E), which incorporated more 5-ethynyl-2′-deoxyuridine (EdU), a proxy for cell proliferation (Figure 6F), compared to the corresponding younger LPs. In addition, cKit+CD133+ LPs were more luminally biased than cKit+CD133− LPs in younger women (Figure 6G; Figure S7B), as demonstrated by a higher proportion of K19+/K14− cells in the organoids. In contrast, older cKit+CD133+ LPs showed a higher proportion of basal K14+/K19− cells (Figure 6H; Figure S7C). Overall, the older cKit+/CD133+ LPs had higher clonogenic activity *in vitro* and gave rise to cells with more MEP/basal-like characteristics, which is consistent with the interpretation that altered LPs give rise to the LEPs that bear the phenotypic hallmarks of aging mammary epithelial cells.

Aged Epithelial Cells Resemble Immortalized Epithelial Cells

Normal epithelial cells must bypass tumor-suppressive barriers to give rise to malignancies. Pre-stasis HMECs can be efficiently immortalized in a two-step process that bypasses Rb function (by *CCND1* expression or *CDKN2A* knockdown) and reactivates telomerase activity (indirectly by MYC expression), while incurring no gross genomic changes (Garbe et al., 2014). Mass cytometry analysis was conducted on 6 immortalized HMEC cell lines and visualized by tSNE. Immortalization via *CCND1* overexpression to bypass stasis was associated with a luminal subtype, whereas knockdown of *CDKN2A* was associated with a basal subtype, and age >60 years, independent of CDKN2A, favored more luminal subtypes to emerge, consistent with our previous report (Lee et al., 2015) (Figures 7A–7C). Strikingly, five of the six immortal cell lines exhibited high expression of the basal markers YAP, Axl, pS6, pPLCγ2, pEGFR, CD44, and pGSK3 (Figures 7D and S7E), which is the same protein cluster observed in the subset of LEPs that accumulated with age (Figures 4B and 5G). Thus, the specific marker expression signatures found in age-emergent LEP subpopulations resemble the immortalized derivatives of older HMECs. This is consistent with the hypothesis that accumulation of altered LPs and LEPs with basal traits during mammary gland aging reflects a breast cancer susceptibility phenotype.

DISCUSSION

At single-cell resolution, these data show the dynamic phenotypic heterogeneity of human mammary epithelia spanning eight decades of life. Phenotypic diversity is present within all cell populations, and *en bloc*-averaged behavior may not represent that of individual cells (Altschuler and Wu, 2010). Mapping the normal diversity of cellular phenotypes within an adult tissue is key to understanding organ-level function and cell-level functionality. Using unbiased computational analyses of 29-parameter mass cytometry, we interrogated epithelial cell lineage diversity in HMEC and uncultured human breast epithelia samples from 57 individuals. We show that the mammary epithelium comprises a complex population of cells residing in phenotypically and functionally diverse states that change with age, and it is more dynamic and heterogeneous than previously perceived (Santagata and Ince, 2014; Taylor-Papadimitriou et al., 1989; Villadsen et al., 2007). This unique data resource provides a repository of single-cell proteomic data combined with cell functional and *in situ* tissue validation to better understand the aging process in mammary epithelia. An important outcome of the high-dimensional comparison, between breast epithelia and primary cultures of HMEC strains, was the excellent correspondence between lineage representation and phenotypes of aging. In general, a challenge of aging research in human tissues is that age-dependent

(E) Intra-sample heterogeneity for each woman is represented graphically by a horizontal bar in which segment lengths represent the proportion of the sample assigned to each cluster, colored accordingly.
(F) Boxplots of cell abundance in each age-related Citrus cluster and its representative tSNE phenotypic projection.
(G) Heatmaps of marker expression of each cluster normalized to LEP from <30-year-old women for clusters A to C and MEP from <30-year-old women for clusters D to G.
(H) The geometric distance was calculated using the square root of the sum of the squared differences between the median of each marker for each subpopulation.
(I) Representative human breast sections immunostained for K14 (red), K19 (green), and DAPI (blue) from a 17-year-old, 36-year-old, and 58-year-old woman (left to right, respectively). Scale bar represents 100 μm.
(J) Plots show classification performance of 171 breast sections from 50 women (<30 years n = 52, >30 < 50 years n = 86, and >50 years n = 33), analyzed using morphometric context with increasing training set size.
(K) Plot shows Citrus classification performance using a training set of 10 women (<30 years n = 5, >50 years n = 5). The black and white circles indicate whether an incorrectly assigned sample was from a peripheral non-tumor mastectomy (P), milk (MK), a tumor (T), or a tissue with no history, respectively. Data are mean ± SEM.
See also Figures S5 and S6.

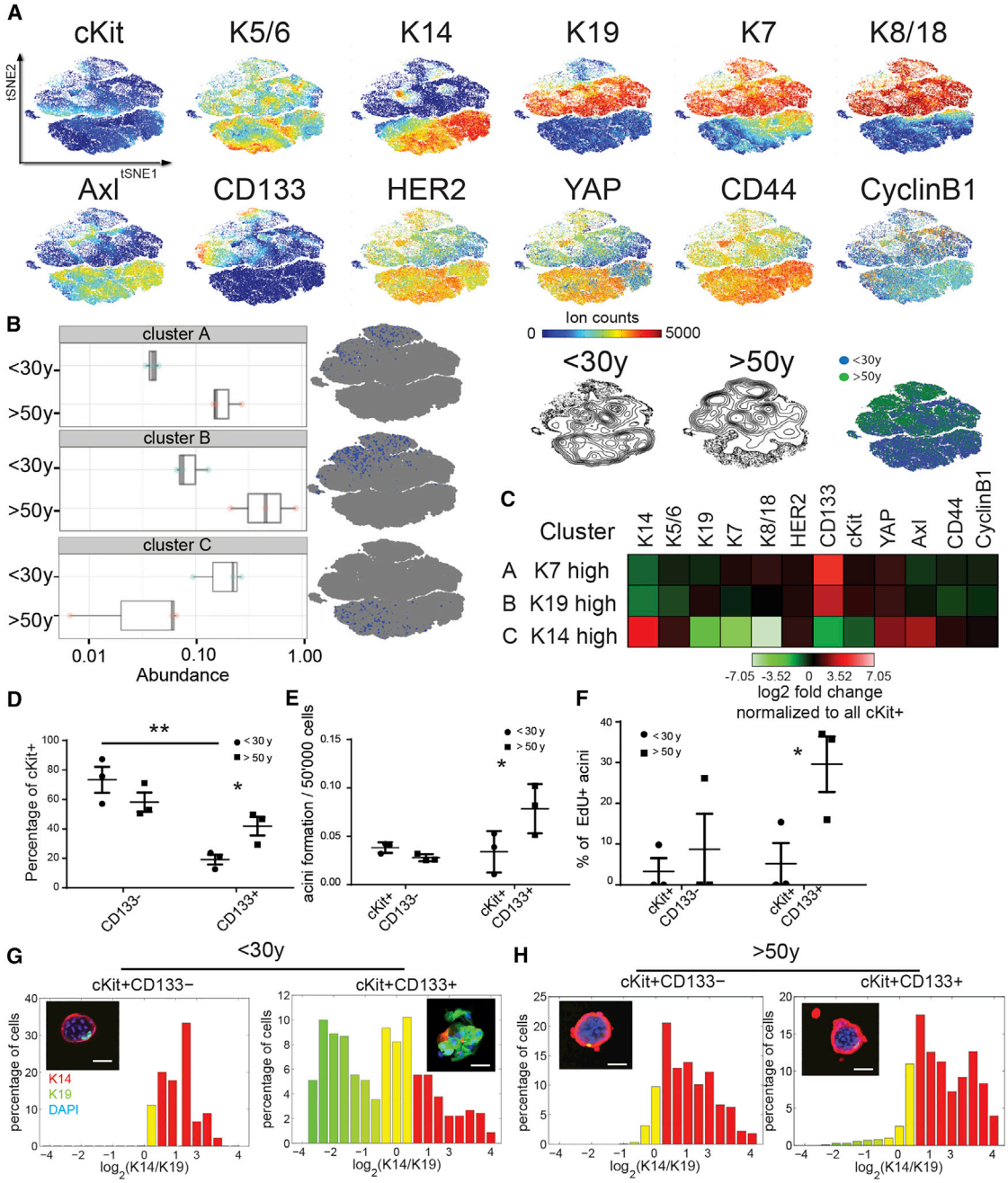

Figure 6. Evidence of Age-Dependent Phenotypic Divergence in HMEC Progenitors

(A) tSNE maps from FACS-enriched HMEC cKit+ progenitors from 3 women <30 years old and 3 women >50 years old (merged and subsampled at 50,000 cells). The lower right tSNE map shows the spatial projection of women <30 years old (blue) and women >50 years old (green).

(B) Boxplots of cell abundance of age-dependent clusters identified with Citrus and their representative tSNE spatial projection.

(C) Heatmaps of marker expression of each cluster compared to the background.

(D) Proportions of cKit+CD133− and cKit+CD133+ as a function of age (n = 3; t test, young cKit+CD133− versus cKit+CD133+ p = 0.0046, and young cKit+CD133+ versus old cKit+CD133+ p = 0.037).

(E) Acini formation potential of cKit+CD133− and cKit+CD133+ in Matrigel/collagen I gels as a function of age (n = 3; t test, p = 0.0123).

(F) Proportions of acini that were incorporating EdU as a function of age. Data are means ± SEM. An acinus was quantified as EdU positive if at least one cell was incorporating EdU (n = 3; t test, p = 0.0452). Data are means ± SEM.

(legend continued on next page)

changes can be cataloged (e.g., transcriptional, proteomic, and biochemical), but it is difficult to study the functional consequences of those changes. As shown here, age-related functional changes in migration, EGF signaling, and 3D colony formation, which were predicted by measurements of the 29 epitopes in breast epithelia, could be explored using primary cultures. Further development of these types of approaches, which combine careful primary HMEC culture with advanced analytical instrumentation and computational analysis, represents a means of accessing human tissue biology in a new and meaningful way.

Older women accumulate mammary multipotent progenitors, the putative cancer cell of origin, with altered differentiation potential, which we and others hypothesize is one of the mechanisms that underlies increased susceptibility to breast cancer with age (Choudhury et al., 2013; Garbe et al., 2012; LaBarge et al., 2016; Proia et al., 2011). Their LEP daughters are not fully lineage committed and acquire a basal phenotype. By using a test set of appropriate size and machine-learning tools, we identified a unique subset of LEPs that accumulate with age, which have skewed differentiation and a basal-like phenotype. These age-emergent LEPs are more adherent to the extracellular matrix (ECM), and they exhibit increased EGF signaling compared to younger LEPs. An unsupervised classification model based on these age-related markers validates the hypothesis that specific age-related changes in LEP subpopulations are good age group predictors. Concomitant age-related changes in LP cells support the concept that the altered stem/progenitor cell populations that accumulate during aging give rise to the age-dependent LEP populations.

The unique constellation of protein levels and modification states that enable classification of mammary epithelia according to age constitutes a signature of aging in the mammary gland. A primary component that distinguishes LEP clusters by age is increased expression of the basal cytokeratin K14 with decreased luminal K19 expression. *In situ* validation of the mass cytometry-derived classification model, by K14 and K19 quantification in tissue sections of normal breast, robustly assigned most breast biopsy samples into their correct age group, further supporting the observation that increased basalness of the LEP compartment is a hallmark characteristic of aging breast tissue. The reduction of LEP migration rate with age, approaching that of MEP, was consistent with increased ECM engagement. Change in the LEP-ECM binding energy is predicted to impair the ability to maintain normal epithelial bilayers (Cerchiari et al., 2015). Indeed, LEP-ECM interactions in older LEP could inhibit the Hippo pathway (Cordenonsi et al., 2011) and activate YAP/TAZ (Naylor et al., 2005), which may help explain our previous observation of increased nuclear YAP in post-menopausal LEP *in vivo* (Pelissier et al., 2014).

Accumulation of stem/progenitor cells with skewed differentiation and function is a hallmark of aging in a number of tissues (Encinas et al., 2011; Garbe et al., 2012; Lugert et al., 2010), and it may confer increased susceptibility to oncogenic events. BRCA1 basal-like breast cancers may originate from cKit-expressing progenitors (Lim et al., 2009; Molyneux et al., 2010). The key changes in the subpopulations of LPs that accumulated with age involved a specific marker signature where cKit, CD133, YAP, and HER2 expression was increased and CD44 expression was decreased. These findings are congruent with the observation that cKit overexpression prevents normal differentiation in murine mammary epithelial progenitors (Regan et al., 2012), and they may explain the accumulation of cKit+ LPs with age. CD133 (Prominin 1), another putative LP marker (Hilton et al., 2014; Raouf et al., 2008), changed the most with age (increased 18.25- and 6.36-fold and decreased 5-fold in protein abundance in each respective cluster compared to <30-year cKit+). In some breast cancers CD133 positivity correlates with a restricted subgroup of tumor stem cells in BRCA1-deficient mammary tumors (Wright et al., 2008). YAP expression in LPs might result in incompletely differentiated LEPs with basal traits (Pelissier et al., 2014). Amplification of HER2 has been shown to play an important role in the development and progression of certain aggressive types of breast cancer (Ménard et al., 2000). Hence, these age-related phenotypes correspond with the cancer-relevant hypothetical effects of cKit, CD133, HER2, and YAP marker expression signature. Older cKit+CD133+ LPs formed basal proliferative colonies in 3D Matrigel/collagen gels, resembling the reported activity of LPs from BRCA1 carriers (Lim et al., 2009). Moreover, hormone treatment in luminal breast cancer reduced estrogen receptor α levels and promoted a cancer stem cell phenotype ($CD133^{high}$ and $CD44^{low}$) (Sansone et al., 2016). This observation correlates well with the fact that augmented $CD133^{high}$ and $CD44^{low}$ cell proportion is associated with an increase in malignancy (Pece et al., 2010) and probably breast cancer risk (Garbe et al., 2012). The cKit+CD133+ LPs are considered potential cells of origin for breast cancer, and we propose that their accumulation with age represents an important facet of age-related susceptibility to breast cancer. Moreover, based on the involvement of these signature proteins (i.e., cKit, CD133, YAP, HER2, and CD44) in a number of breast cancer-relevant contexts, it is tempting to speculate that their dysregulation in older LPs also is related to increased susceptibility to breast cancer with age.

We identified shared expression signatures between age-emergent luminal cell subpopulations and immortalized derivatives of older HMECs, which have overcome at least two major barriers to tumor progression. Five of the six immortal cell lines exhibited high expression of the core markers (YAP, Axl, pS6, pPLCγ2, pEGFR, CD44, and pGSK3 [inactivated when phosphorylated]), which defines a putative signature of transformed HMECs that was also part of the core changes in normally aging LEPs. All of those core markers were reported to have a role in breast cancer progression (Gjerdrum et al., 2010; Kassis et al., 1999; Kim et al., 2015; Ko et al., 2016; Louderbough and Schroeder, 2011; Masuda et al., 2012; Yanai et al., 2015).

(G and H) Histograms represent $\log_2$-transformed ratios of K14 to K19 protein expression in single cells of acini (G) from a representative woman <30 years old (240L, 19 years) and (H) from a representative woman >50 years old (029, 68 years). Histograms are heat mapped to indicate the phenotypes of K14−/K19+ LEP (green), K14+/K19+ progenitors (yellow), and K14+/K19− MEP (red). Insets show representative HMEC organoids immunostained for K14 (red), K19 (green), and DAPI (blue). Scale bar represents 50 μm.
See also Figure S7.

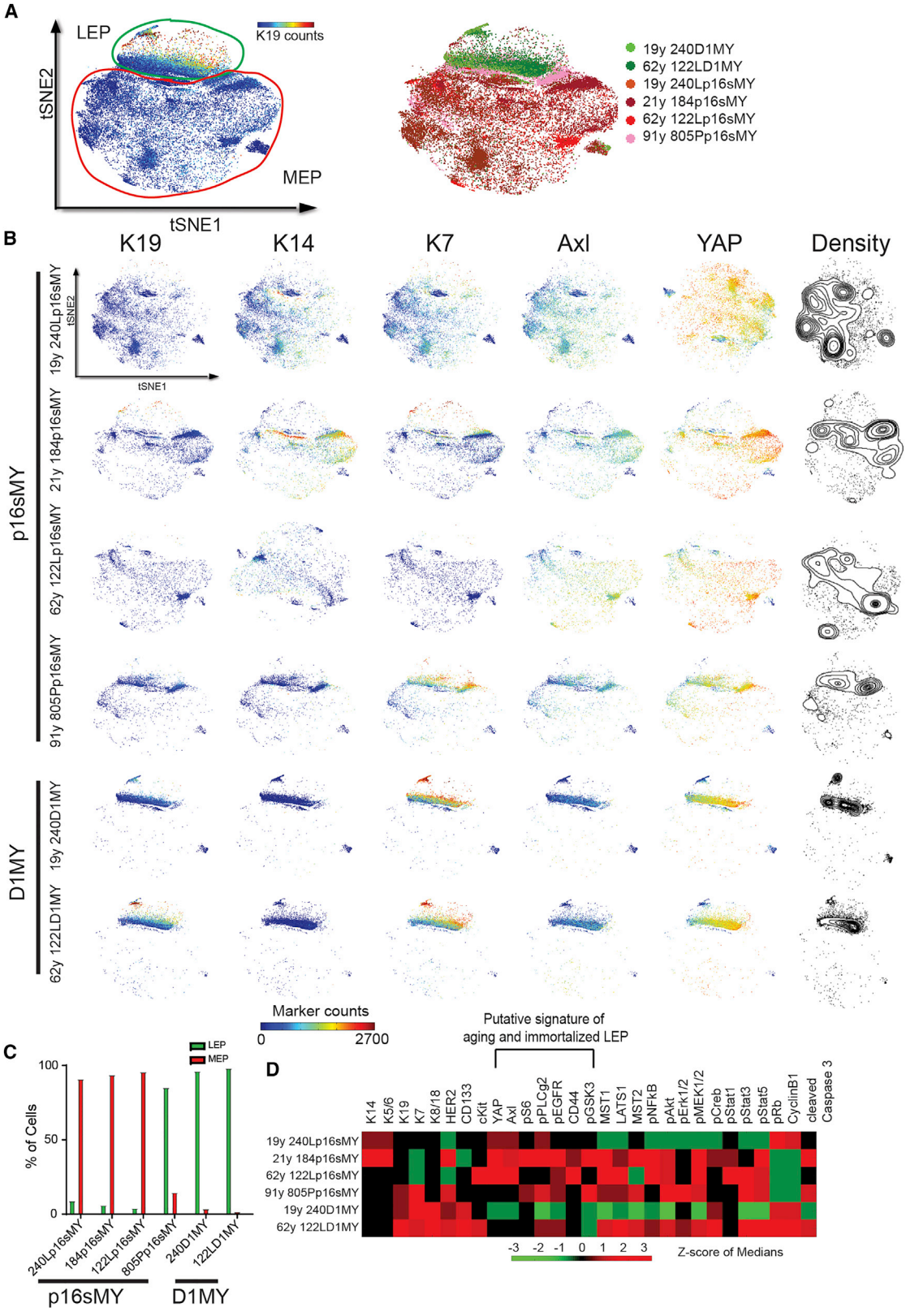

(legend on next page)

Machine-learning algorithms that we used to validate the aging signature incorrectly classified nine young and middle-aged primary strains as old. Six of those strains were from women with mutations in BRCA1 or ATM, or they were derived from normal-appearing tissue that was peripheral to a tumor, or they were the normal cells cultured out directly from a tumor. It is tempting to speculate that epithelia in women who are innately at higher risk will exhibit an effective age that is older than the chronological age. A similar idea was proposed by epidemiologists that took into account breast tissue age, using only measures of hormones and childbirths (Pike et al., 1983). Here we provide evidence of a cell- and molecular-level manifestation of this concept. A biological explanation of advanced effective age in epithelia could be that molecular states that are associated with risk exert field effects (Deng et al., 1996), which alter the epithelia through a dynamic and reciprocal communication between stroma and epithelia. Ultimately, further investigation may lead to the development of novel approaches for prevention, patient stratification, and therapeutic interventions to combat age-associated breast cancers.

EXPERIMENTAL PROCEDURES

Cell Culture and Uncultured Breast Epithelia

All cell culture was in M87A medium with 0.1 nM oxytocin (X) and cholera toxin (CT) at 0.5 ng/mL (Garbe et al., 2009). Primary HMEC strains were generated and maintained as described (Labarge et al., 2013). All tissues were obtained with proper oversight from the Lawrence Berkeley National Laboratory institutional review board. Breast tissue from reduction mammoplasty was manually dissected to enrich for gland-containing material. Stromal tissue was separated from epithelial fragments using a brief treatment with collagenase. The uncultured breast epithelia samples were dissociated as single cells with trypsin. All the pre-stasis HMEC strains were used at fourth passage (Table S1). Fibroblasts were removed and collected separately by differential trypsinization during the first passage. During the functional assay, HMECs were treated with EGF (Sigma E-9644, 0.1 μg/mL) and sodium orthovanadate (Sigma 13721-39-6, 12.5 mM) for 1 hr. Samples were harvested with TrypLE, fixed with 1.6% paraformaldehyde (PFA) for 10 min at room temperature (RT), and frozen as a pellet at −80°C for further analysis.

Antibodies Used for Mass Cytometry Analysis

Antibodies were obtained in carrier protein-free PBS and then prepared using the MaxPAR antibody conjugation kit (Fluidigm), according to the manufacturer's protocol. After determining the percentage yield by measurement of absorbance at 280 nm, the metal-labeled antibodies were diluted in Candor PBS Antibody Stabilization solution (Candor Bioscience) for long-term storage at 4°C (Table S2). Antibodies were titrated and validated beforehand using both positive and negative cell controls (Table S2; Figure S1). Extensive antibody validation has been performed and published previously (Chevrier et al., 2017; Giesen et al., 2014).

Cell Barcoding and Antibody Staining

HMEC strains were incubated with cisplatin (WR International, Cat# 89150-634, 25 μM) for 1 min to assess cell viability (Fienberg et al., 2012), fixed in 1.6% PFA for 10 min at RT, and washed once with Cell Staining Media (CSM, PBS with 0.5% BSA and 0.02% NaN_3 with 0.03% saponin). The cells were then resuspended in PBS, and DMSO stocks of the barcoding reagent were added as described (Bodenmiller et al., 2012; Zivanovic et al., 2014). The cells were incubated at RT for 30 min, washed three times with CSM, and then pooled into a single FACS tube for staining with metal-labeled antibodies for 1 hr at RT. A staining volume of 800 μL was used (~30 × 10^6 cells/mL). After antibody staining, the cells were washed twice with CSM and once with PBS, and then incubated for 20 min at RT or overnight at 4°C with an iridium-containing intercalator (DVS Sciences) in PBS with 1.6% PFA. The cells were then washed three times with CSM and once with PBS, diluted with water to ~10^6 cells/mL, and filtered through a 40-μm membrane just before analysis by mass cytometry.

Data Analysis

The scale used before analysis is the arcsinh with the cofactor of 5 (x_transf = asinh(x/5)). After gating out viable and iridium-labeled events, the data were analyzed by applying tSNE. This non-linear dimensionally reduction technique is implemented via Barnes-Hut approximations in the MATLAB toolbox *cyt* (Amir et al., 2013). We used the default parameters (initial dimensions, 110; perplexity, 30; and theta, 0.5). Each sample contained 20,000 cells, when merged, 320,000 cells from HMEC <30 years, 260,000 cells from HMEC >30 < 50 years, and 300,000 cells from HMEC >50 years. In tSNE, each cell is represented as a point in high-dimensional space. Each dimension is one parameter (the expression level of each protein in our case).

The unsupervised PhenoGraph algorithm in *cyt* has been used to group cells that are phenotypically similar and cluster these subpopulations using modularity optimization (Levine et al., 2015). tSNE and PhenoGraph were performed only on surface markers. A number of neighbors of 800 was selected. This parameter was chosen based on prior knowledge of the underlying cell types. Lower values for nearest neighbors result in an overclustering and higher values an underclustering.

The Citrus toolbox in R was used to identify clusters that changed in abundance with age (Bruggner et al., 2014) in an unsupervised manner. Therefore, clusters were identified using a hierarchical clustering and linked to clinical data for characterization. The minimal selected cluster size was 0.1% of the total analyzed data. Stratifying clusters were learned by using regularized unsupervised learning methods. Heatmaps were obtained with MATLAB and Cytobank. The results were reproduced with strains obtained from reduction mammoplasties (RMs) only.

Classification

Citrus was implemented in the PAM package for R and used nearest shrunken centroids as a predictive model to identify properties that are predictive of sample class. The prediction model was based on the initial training data model. Therefore, new samples were mapped and later assigned to the initial clusters for prediction. Using a training set of 5 HMECs from women <30 years old and 5 women >50 years old (n = 10), Citrus efficiently assigned most of the test set to young or old. The training set was changed to n = 8 and to n = 12 with similar efficiency. After randomization of the training set, the classification failed. The R code is found in the Supplemental Experimental Procedures.

Classification Using Morphometric Context

Each image was represented as its Cellular Morphometric Context (Chang et al., 2013), which was constructed as the histogram of cellular morphometric subtypes derived from the cellular morphometric features (K14/K19 signals) through K-Means (dictionary size = 1,024). Homogeneous kernel map (Vedaldi and Zisserman, 2012) was then applied on the Cellular Morphometric

Figure 7. Aged Epithelia Resemble Immortalized Epithelial Cells

(A) tSNE map of immortalized HMECs (left, merged, 6,000 cells per sample, n = 6). Right: each color represents a strain.
(B) Five selected markers are shown (K19, K4, K7, Axl, and YAP), with knockdown of CDKN2A: p16sMY and overexpression of CCND1: D1MY.
(C) Plots show percentage of LEP and MEP in each strain according to the gating strategy.
(D) Heatmap of *Z* score of median of marker expression of each strain.
See also Figure S7.

Context representation, so that linear support vector machine (SVM) (Yang et al., 2009) could be adopted for efficient and effective differentiation among age groups.

Statistical Analysis

GraphPad Prism, R, and MATLAB were used for all statistical analyses. Standard linear regression and t tests were used. Grouped analyses were performed with Bonferroni-Holm correction for multiple comparisons. Significance was established when $*p < 0.05$, $**p < 0.01$, and $***p < 0.001$.

DATA AND SOFTWARE AVAILABILITY

The accession number for the CyTOF data reported in this paper is Mendeley Data: https://doi.org/10.17632/j7mrbgt3hh.1.

SUPPLEMENTAL INFORMATION

Supplemental Information includes Supplemental Experimental Procedures, seven figures, and two tables and can be found with this article online at https://doi.org/10.1016/j.celrep.2018.03.114.

ACKNOWLEDGMENTS

We thank Dr. Thibault Vatter, Dr. Robert Bruggner, and Dr. Adeeb Rahman for expert advice. The imaging and FACS were performed at the Molecular Imaging Center (MIC) at the University of Bergen. F.A.P.V. was supported by a University of Bergen pre-doctoral fellowship and travel grants. D.S. was supported by the Forschungskredit of the University of Zurich (grant FK-74419-01-01) and the BioEntrepreneur-Fellowship of the University of Zurich (BIOEF-17-001). J.B.L. is supported by grants from the Research Council of Norway (240130), Centres of Excellence funding scheme (223250), and Helse Vest Health Authority (911794). M.A.L. is supported by NIH R00AG033176 and R01AG040081 and a Congressionally Directed Medical Research Programs Breast Cancer Research Program Era of Hope Scholar Award BC141351. B.B. is supported by the Swiss National Science Foundation (SNSF) R'Equip grant 316030-139220, a SNSF Assistant Professorship grant PP00P3-144874, the PhosphonetPPM SystemsX grant (UC4 DK108132), and funding from the European Research Council (ERC) under the European Union's Seventh Framework Programme (FP/2007-2013)/ERC Grant Agreement 336921. D.S. was supported by a Forschungskredit Fellowship of the University of Zurich.

AUTHOR CONTRIBUTIONS

F.A.P.V., J.B.L., B.B., and M.A.L. designed the research. F.A.P.V. performed experiments. F.A.P.V., D.S., H.C., A.D.B., J.K.L., and B.P. analyzed the data and provided conceptual input. M.R.S., A.D.B., and M.A.L. provided cell strains, tissue sections, and other key reagents. B.B. provided the CyTOF platform. F.A.P.V., D.S., B.B., J.B.L., and M.A.L. wrote the manuscript.

DECLARATION OF INTERESTS

The authors declare no competing interests.

Received: October 27, 2017
Revised: January 19, 2018
Accepted: March 25, 2018
Published: April 24, 2018

REFERENCES

Altschuler, S.J., and Wu, L.F. (2010). Cellular heterogeneity: do differences make a difference? Cell *141*, 559–563.

Amir, E.D., Davis, K.L., Tadmor, M.D., Simonds, E.F., Levine, J.H., Bendall, S.C., Shenfeld, D.K., Krishnaswamy, S., Nolan, G.P., and Pe'er, D. (2013). viSNE enables visualization of high dimensional single-cell data and reveals phenotypic heterogeneity of leukemia. Nat. Biotechnol. *31*, 545–552.

Bandura, D.R., Baranov, V.I., Ornatsky, O.I., Antonov, A., Kinach, R., Lou, X., Pavlov, S., Vorobiev, S., Dick, J.E., and Tanner, S.D. (2009). Mass cytometry: technique for real time single cell multitarget immunoassay based on inductively coupled plasma time-of-flight mass spectrometry. Anal. Chem. *81*, 6813–6822.

Bergstraesser, L.M., Srinivasan, G., Jones, J.C., Stahl, S., and Weitzman, S.A. (1995). Expression of hemidesmosomes and component proteins is lost by invasive breast cancer cells. Am. J. Pathol. *147*, 1823–1839.

Biteau, B., Hochmuth, C.E., and Jasper, H. (2008). JNK activity in somatic stem cells causes loss of tissue homeostasis in the aging Drosophila gut. Cell Stem Cell *3*, 442–455.

Bodenmiller, B., Zunder, E.R., Finck, R., Chen, T.J., Savig, E.S., Bruggner, R.V., Simonds, E.F., Bendall, S.C., Sachs, K., Krutzik, P.O., and Nolan, G.P. (2012). Multiplexed mass cytometry profiling of cellular states perturbed by small-molecule regulators. Nat. Biotechnol. *30*, 858–867.

Brantley, D.M., Chen, C.L., Muraoka, R.S., Bushdid, P.B., Bradberry, J.L., Kittrell, F., Medina, D., Matrisian, L.M., Kerr, L.D., and Yull, F.E. (2001). Nuclear factor-kappaB (NF-kappaB) regulates proliferation and branching in mouse mammary epithelium. Mol. Biol. Cell *12*, 1445–1455.

Bruggner, R.V., Bodenmiller, B., Dill, D.L., Tibshirani, R.J., and Nolan, G.P. (2014). Automated identification of stratifying signatures in cellular subpopulations. Proc. Natl. Acad. Sci. USA *111*, E2770–E2777.

Cerchiari, A.E., Garbe, J.C., Jee, N.Y., Todhunter, M.E., Broaders, K.E., Peehl, D.M., Desai, T.A., LaBarge, M.A., Thomson, M., and Gartner, Z.J. (2015). A strategy for tissue self-organization that is robust to cellular heterogeneity and plasticity. Proc. Natl. Acad. Sci. USA *112*, 2287–2292.

Chang, H., Borowsky, A., Spellman, P., and Parvin, B. (2013). Classification of Tumor Histology via Morphometric Context. In Proceedings of the Conference on Computer Vision and Pattern Recognition (IEEE), pp. 2203–2210.

Chen, Q., Zhang, N., Gray, R.S., Li, H., Ewald, A.J., Zahnow, C.A., and Pan, D. (2014). A temporal requirement for Hippo signaling in mammary gland differentiation, growth, and tumorigenesis. Genes Dev. *28*, 432–437.

Chevrier, S., Levine, J.H., Zanotelli, V.R.T., Silina, K., Schulz, D., Bacac, M., Ries, C.H., Ailles, L., Jewett, M.A.S., Moch, H., et al. (2017). An Immune Atlas of Clear Cell Renal Cell Carcinoma. Cell *169*, 736–749.e18.

Choudhury, S., Almendro, V., Merino, V.F., Wu, Z., Maruyama, R., Su, Y., Martins, F.C., Fackler, M.J., Bessarabova, M., Kowalczyk, A., et al. (2013). Molecular profiling of human mammary gland links breast cancer risk to a p27(+) cell population with progenitor characteristics. Cell Stem Cell *13*, 117–130.

Cordenonsi, M., Zanconato, F., Azzolin, L., Forcato, M., Rosato, A., Frasson, C., Inui, M., Montagner, M., Parenti, A.R., Poletti, A., et al. (2011). The Hippo transducer TAZ confers cancer stem cell-related traits on breast cancer cells. Cell *147*, 759–772.

Deng, G., Lu, Y., Zlotnikov, G., Thor, A.D., and Smith, H.S. (1996). Loss of heterozygosity in normal tissue adjacent to breast carcinomas. Science *274*, 2057–2059.

dos Santos, C.O., Rebbeck, C., Rozhkova, E., Valentine, A., Samuels, A., Kadiri, L.R., Osten, P., Harris, E.Y., Uren, P.J., Smith, A.D., and Hannon, G.J. (2013). Molecular hierarchy of mammary differentiation yields refined markers of mammary stem cells. Proc. Natl. Acad. Sci. USA *110*, 7123–7130.

Encinas, J.M., Michurina, T.V., Peunova, N., Park, J.H., Tordo, J., Peterson, D.A., Fishell, G., Koulakov, A., and Enikolopov, G. (2011). Division-coupled astrocytic differentiation and age-related depletion of neural stem cells in the adult hippocampus. Cell Stem Cell *8*, 566–579.

Fienberg, H.G., Simonds, E.F., Fantl, W.J., Nolan, G.P., and Bodenmiller, B. (2012). A platinum-based covalent viability reagent for single-cell mass cytometry. Cytometry A *81*, 467–475.

Garbe, J.C., Bhattacharya, S., Merchant, B., Bassett, E., Swisshelm, K., Feiler, H.S., Wyrobek, A.J., and Stampfer, M.R. (2009). Molecular distinctions between stasis and telomere attrition senescence barriers shown by long-term culture of normal human mammary epithelial cells. Cancer Res. *69*, 7557–7568.

Garbe, J.C., Pepin, F., Pelissier, F.A., Sputova, K., Fridriksdottir, A.J., Guo, D.E., Villadsen, R., Park, M., Petersen, O.W., Borowsky, A.D., et al. (2012). Accumulation of multipotent progenitors with a basal differentiation bias during aging of human mammary epithelia. Cancer Res. *72*, 3687–3701.

Garbe, J.C., Vrba, L., Sputova, K., Fuchs, L., Novak, P., Brothman, A.R., Jackson, M., Chin, K., LaBarge, M.A., Watts, G., et al. (2014). Immortalization of normal human mammary epithelial cells in two steps by direct targeting of senescence barriers does not require gross genomic alterations. Cell Cycle *13*, 3423–3435.

Giacinti, C., and Giordano, A. (2006). RB and cell cycle progression. Oncogene *25*, 5220–5227.

Giesen, C., Wang, H.A., Schapiro, D., Zivanovic, N., Jacobs, A., Hattendorf, B., Schüffler, P.J., Grolimund, D., Buhmann, J.M., Brandt, S., et al. (2014). Highly multiplexed imaging of tumor tissues with subcellular resolution by mass cytometry. Nat. Methods *11*, 417–422.

Gjerdrum, C., Tiron, C., Høiby, T., Stefansson, I., Haugen, H., Sandal, T., Collett, K., Li, S., McCormack, E., Gjertsen, B.T., et al. (2010). Axl is an essential epithelial-to-mesenchymal transition-induced regulator of breast cancer metastasis and patient survival. Proc. Natl. Acad. Sci. USA *107*, 1124–1129.

Härdle, W., and Simar, L. (2007). Applied multivariate statistical analysis, *Volume 22007* (Springer).

Hilton, H.N., Santucci, N., Silvestri, A., Kantimm, S., Huschtscha, L.I., Graham, J.D., and Clarke, C.L. (2014). Progesterone stimulates progenitor cells in normal human breast and breast cancer cells. Breast Cancer Res. Treat. *143*, 423–433.

Kassis, J., Moellinger, J., Lo, H., Greenberg, N.M., Kim, H.G., and Wells, A. (1999). A role for phospholipase C-gamma-mediated signaling in tumor cell invasion. Clin. Cancer Res. *5*, 2251–2260.

Kim, H.M., Jung, W.H., and Koo, J.S. (2015). Expression of Yes-associated protein (YAP) in metastatic breast cancer. Int. J. Clin. Exp. Pathol. *8*, 11248–11257.

Ko, H.W., Lee, H.H., Huo, L., Xia, W., Yang, C.C., Hsu, J.L., Li, L.Y., Lai, C.C., Chan, L.C., Cheng, C.C., et al. (2016). GSK3β inactivation promotes the oncogenic functions of EZH2 and enhances methylation of H3K27 in human breast cancers. Oncotarget *7*, 57131–57144.

LaBarge, M.A., Petersen, O.W., and Bissell, M.J. (2007). Of microenvironments and mammary stem cells. Stem Cell Rev. *3*, 137–146.

Labarge, M.A., Garbe, J.C., and Stampfer, M.R. (2013). Processing of human reduction mammoplasty and mastectomy tissues for cell culture. J. Vis. Exp. (*71*), 50011.

LaBarge, M.A., Mora-Blanco, E.L., Samson, S., and Miyano, M. (2016). Breast Cancer beyond the Age of Mutation. Gerontology *62*, 434–442.

Lee, J.K., Garbe, J.C., Vrba, L., Miyano, M., Futscher, B.W., Stampfer, M.R., and LaBarge, M.A. (2015). Age and the means of bypassing stasis influence the intrinsic subtype of immortalized human mammary epithelial cells. Front. Cell Dev. Biol. *3*, 13.

Levine, J.H., Simonds, E.F., Bendall, S.C., Davis, K.L., Amir, E.D., Tadmor, M.D., Litvin, O., Fienberg, H.G., Jager, A., Zunder, E.R., et al. (2015). Data-Driven Phenotypic Dissection of AML Reveals Progenitor-like Cells that Correlate with Prognosis. Cell *162*, 184–197.

Lim, E., Vaillant, F., Wu, D., Forrest, N.C., Pal, B., Hart, A.H., Asselin-Labat, M.L., Gyorki, D.E., Ward, T., Partanen, A., et al.; kConFab (2009). Aberrant luminal progenitors as the candidate target population for basal tumor development in BRCA1 mutation carriers. Nat. Med. *15*, 907–913.

Louderbough, J.M., and Schroeder, J.A. (2011). Understanding the dual nature of CD44 in breast cancer progression. Mol. Cancer Res. *9*, 1573–1586.

Lugert, S., Basak, O., Knuckles, P., Haussler, U., Fabel, K., Götz, M., Haas, C.A., Kempermann, G., Taylor, V., and Giachino, C. (2010). Quiescent and active hippocampal neural stem cells with distinct morphologies respond selectively to physiological and pathological stimuli and aging. Cell Stem Cell *6*, 445–456.

Mansilla, E., Díaz Aquino, V., Zambón, D., Marin, G.H., Mártire, K., Roque, G., Ichim, T., Riordan, N.H., Patel, A., Sturla, F., et al. (2011). Could metabolic syndrome, lipodystrophy, and aging be mesenchymal stem cell exhaustion syndromes? Stem Cells Int. *2011*, 943216.

Masuda, H., Zhang, D., Bartholomeusz, C., Doihara, H., Hortobagyi, G.N., and Ueno, N.T. (2012). Role of epidermal growth factor receptor in breast cancer. Breast Cancer Res. Treat. *136*, 331–345.

Ménard, S., Tagliabue, E., Campiglio, M., and Pupa, S.M. (2000). Role of HER2 gene overexpression in breast carcinoma. J. Cell. Physiol. *182*, 150–162.

Molyneux, G., Geyer, F.C., Magnay, F.A., McCarthy, A., Kendrick, H., Natrajan, R., Mackay, A., Grigoriadis, A., Tutt, A., Ashworth, A., et al. (2010). BRCA1 basal-like breast cancers originate from luminal epithelial progenitors and not from basal stem cells. Cell Stem Cell *7*, 403–417.

Naylor, M.J., Li, N., Cheung, J., Lowe, E.T., Lambert, E., Marlow, R., Wang, P., Schatzmann, F., Wintermantel, T., Schüetz, G., et al. (2005). Ablation of beta1 integrin in mammary epithelium reveals a key role for integrin in glandular morphogenesis and differentiation. J. Cell Biol. *171*, 717–728.

Pasic, L., Eisinger-Mathason, T.S., Velayudhan, B.T., Moskaluk, C.A., Brenin, D.R., Macara, I.G., and Lannigan, D.A. (2011). Sustained activation of the HER1-ERK1/2-RSK signaling pathway controls myoepithelial cell fate in human mammary tissue. Genes Dev. *25*, 1641–1653.

Pece, S., Tosoni, D., Confalonieri, S., Mazzarol, G., Vecchi, M., Ronzoni, S., Bernard, L., Viale, G., Pelicci, P.G., and Di Fiore, P.P. (2010). Biological and molecular heterogeneity of breast cancers correlates with their cancer stem cell content. Cell *140*, 62–73.

Pelissier, F.A., Garbe, J.C., Ananthanarayanan, B., Miyano, M., Lin, C., Jokela, T., Kumar, S., Stampfer, M.R., Lorens, J.B., and LaBarge, M.A. (2014). Age-related dysfunction in mechanotransduction impairs differentiation of human mammary epithelial progenitors. Cell Rep. *7*, 1926–1939.

Pike, M.C., Krailo, M.D., Henderson, B.E., Casagrande, J.T., and Hoel, D.G. (1983). 'Hormonal' risk factors, 'breast tissue age' and the age-incidence of breast cancer. Nature *303*, 767–770.

Pitelka, D.R., Hamamoto, S.T., Duafala, J.G., and Nemanic, M.K. (1973). Cell contacts in the mouse mammary gland. I. Normal gland in postnatal development and the secretory cycle. J. Cell Biol. *56*, 797–818.

Proia, T.A., Keller, P.J., Gupta, P.B., Klebba, I., Jones, A.D., Sedic, M., Gilmore, H., Tung, N., Naber, S.P., Schnitt, S., et al. (2011). Genetic predisposition directs breast cancer phenotype by dictating progenitor cell fate. Cell Stem Cell *8*, 149–163.

Raouf, A., Zhao, Y., To, K., Stingl, J., Delaney, A., Barbara, M., Iscove, N., Jones, S., McKinney, S., Emerman, J., et al. (2008). Transcriptome analysis of the normal human mammary cell commitment and differentiation process. Cell Stem Cell *3*, 109–118.

Regan, J.L., Kendrick, H., Magnay, F.A., Vafaizadeh, V., Groner, B., and Smalley, M.J. (2012). c-Kit is required for growth and survival of the cells of origin of Brca1-mutation-associated breast cancer. Oncogene *31*, 869–883.

Sansone, P., Ceccarelli, C., Berishaj, M., Chang, Q., Rajasekhar, V.K., Perna, F., Bowman, R.L., Vidone, M., Daly, L., Nnoli, J., et al. (2016). Self-renewal of CD133(hi) cells by IL6/Notch3 signalling regulates endocrine resistance in metastatic breast cancer. Nat. Commun. *7*, 10442.

Santagata, S., and Ince, T.A. (2014). Normal cell phenotypes of breast epithelial cells provide the foundation of a breast cancer taxonomy. Expert Rev. Anticancer Ther. *14*, 1385–1389.

Sharpless, N.E., and DePinho, R.A. (2007). How stem cells age and why this makes us grow old. Nat. Rev. Mol. Cell Biol. *8*, 703–713.

Skibinski, A., Breindel, J.L., Prat, A., Galván, P., Smith, E., Rolfs, A., Gupta, P.B., LaBaer, J., and Kuperwasser, C. (2014). The Hippo transducer TAZ interacts with the SWI/SNF complex to regulate breast epithelial lineage commitment. Cell Rep. *6*, 1059–1072.

Stephens, P.J., Tarpey, P.S., Davies, H., Van Loo, P., Greenman, C., Wedge, D.C., Nik-Zainal, S., Martin, S., Varela, I., Bignell, G.R., et al.; Oslo Breast Cancer Consortium (OSBREAC) (2012). The landscape of cancer genes and mutational processes in breast cancer. Nature *486*, 400–404.

Taylor-Papadimitriou, J., Stampfer, M., Bartek, J., Lewis, A., Boshell, M., Lane, E.B., and Leigh, I.M. (1989). Keratin expression in human mammary epithelial

cells cultured from normal and malignant tissue: relation to in vivo phenotypes and influence of medium. J. Cell Sci. *94*, 403–413.

Vedaldi, A., and Zisserman, A. (2012). Efficient additive kernels via explicit feature maps. IEEE Trans. Pattern Anal. Mach. Intell. *34*, 480–492.

Villadsen, R., Fridriksdottir, A.J., Rønnov-Jessen, L., Gudjonsson, T., Rank, F., LaBarge, M.A., Bissell, M.J., and Petersen, O.W. (2007). Evidence for a stem cell hierarchy in the adult human breast. J. Cell Biol. *177*, 87–101.

Wright, M.H., Calcagno, A.M., Salcido, C.D., Carlson, M.D., Ambudkar, S.V., and Varticovski, L. (2008). Brca1 breast tumors contain distinct CD44+/CD24- and CD133+ cells with cancer stem cell characteristics. Breast Cancer Res. *10*, R10.

Yanai, A., Inoue, N., Yagi, T., Nishimukai, A., Miyagawa, Y., Murase, K., Imamura, M., Enomoto, Y., Takatsuka, Y., Watanabe, T., et al. (2015). Activation of mTOR/S6K But Not MAPK Pathways Might Be Associated With High Ki-67, ER(+), and HER2(-) Breast Cancer. Clin. Breast Cancer *15*, 197–203.

Yang, J., Yu, K., Gong, Y., and Huang, T. (2009). Linear Spatial Pyramid Matching Using Sparse Coding for Image Classification. In Proceedings of the Conference on Computer Vision and Pattern Recognition (IEEE), pp. 1794–1801.

Zivanovic, N., Jacobs, A., and Bodenmiller, B. (2014). A practical guide to multiplexed mass cytometry. Curr. Top. Microbiol. Immunol. *377*, 95–109.

Cell Reports, Volume *23*

Supplemental Information

High-Dimensional Phenotyping Identifies Age-Emergent Cells in Human Mammary Epithelia

Fanny A. Pelissier Vatter, Denis Schapiro, Hang Chang, Alexander D. Borowsky, Jonathan K. Lee, Bahram Parvin, Martha R. Stampfer, Mark A. LaBarge, Bernd Bodenmiller, and James B. Lorens

Supplemental Information

Women <30y			
Sample	Age, y	Source	Known characteristics/ pathology notes
48R	16	RM	African-American
160	16	RM	
407P	19	P	IDC, lymph node+, ER+, PR+
240L	19	RM	Mildly hyperplastic
168R	19	RM	African-American
399E	20	RM	Benign
184	21	RM	
356E	21	RM	Normal
001P	24	P	IDC, lymph node-
123	27	RM	African-American, mammary hyperplasis
195L	27	RM	
97	27	RM	
51L	28	RM	Mild periductal mastitis (R+L) focal microcalcification (R.)
172L	28	RM	Minimal phase of fibrocystic disease
676P	29	P	
124	29	RM	

Women >30y and <50y			
Sample	Age, y	Source	Known characteristics/ pathology notes
42P	30	P	IDC, lymph node-
169L	35	RM	
90P	36	P	BRCA-1 mut (185delAG)
250MK	37	Milk	
100P	39	P	Nonivasive ductal carcinoma, ER-, PR-
6	40	RM	
245AT	41	RM	ATM heterozygote, tissue was clinically normal tissue
173P	45	P	
173T	45	Tumor	IDC, ER-, PR-
208	45	RM	
2	46	RM	
60R	47	RM	
30	49	RM	

Women >50y			
Sample	Age, y	Source	Known characteristics/ pathology notes
178R	51	RM	
191L	56	RM	Slight fibrocystic disease, hypertrophy, stromal fibrosis and adenosis present in mammary parenchyma
117R	56	RM	Patchy stromal fibrosis (R.), fibrocystic disease (L.)
335R	58	P	Infiltrating adenocarcinoma, ER+, PR+/-
153L	60	RM	Benign fibrocystic disease
639P	60	P	
122L	62	RM	Fibrocystic disease, hypertrophy, apocrine metaplasia of ductal epithelium, cystic dilatia of ducts, and focal areas of intraductal hyperplasia
881P	65	P	
96R	66	RM	Slight focal fibrocystic change
29	68	RM	
353P	72	P	Colloid (mucinous) carcinoma, ER+/-, PR-
429ER	72	RM	
464P	80	P	
451P	83	P	
805P	91	P	

Breast Epithelia Samples		
Sample	**Age, y**	**Source**
404EB	19	RM
399E	20	RM
472ER	21	RM
620EL	22	RM
483EHRA	26	RM
400ER	27	RM
437E	29	RM
334ER	55	RM
337ER	57	RM
563HRR	61	RM
395C	62	RM
429EL	72	RM
368E	73	RM

Table S1. HMEC and uncultured breast epithelia samples (Related to Figure 1). HMEC strains and uncultured breast epithelia samples were derived from reduction mammoplasty (RM), peripheral non-tumor regions from mastectomy (P) tissues, milk fluids (Milk) and a tumor (T). The name of the HMEC strain, the age at the time of surgery and the characteristics are indicated.

Isotope	Antigen	Antibody raised against	Pathway	References	Clone	Supplier	Final Concentration ug/mL
ER 170	K14	Total	Myoepithelial marker	(Villadsen et al., 2007)	polyclonal	Thermo	0.25
PR 141	K5/6	Total	Myoepithelial marker	(LaBarge et al., 2007)	D5	Millipore	4
DY 163	K19	Total	Luminal marker	(Villadsen et al., 2007)	TromaIII	DSHB	2
DY164	K7	Total	Luminal marker	(Taylor-Papadimitriou et al., 1989)	RCK105	BD	0.5
YB 174	K8/18	Total	Luminal marker	(Villadsen et al., 2007)	C51	CST	2
YB 173	CD133	Total, epitope 1	Luminal marker	(dos Santos et al., 2013)	AC133	Miltenyi	0.5
GD 161	cKit	Total	Progenitor marker	(Lim et al., 2009; Regan etal., 2012)	104D2	Biolegend	4
ER 168	Axl	Total	Stemness	(Asiedu et al., 2014)	1H12	BergenBio	4
GD 160	CD44	Total, surface	Stemness, migration	(Hebbard et al., 2000; Louderbough et al., 2011)	IM7	BD	0.1
HO 165	HER2	C terminal 1242-1255	Proliferation	(Rubin, Yarden, 2001; Yarden, 2011)	3B5	BD	4
ER 167	YAP	C terminal 379-407	Hippo	(Zhao et al., 2010; Vlug et al., 2013)	H9	Santa Cruz	4
ND148	MST1	aa475-505	Hippo	(Zhao et al., 2010)	polyclonal	LS-Bio	8
SM149	LATS1	N-terminus	Hippo	(Zhao et al., 2010)	polyclonal	LS-Bio	8
DY 162	MST2	Total	Hippo	(Zhao et al., 2010)	polyclonal	LS-Bio	8
LA 139	pCreb	pS133	Survival	(Dietze et al., 2005)	J151-21	BD	4
ND 144	pMEK1/2	pS221	Myoepithelial contractility	(Pasic et al., 2011)	166F8	CST	6
ND 145	pStat3	pY705	Involution	(Haricharan and Li, 2014)	4/pStat3	BD	4
ND 146	pStat5	pY694	Lobuloalveolar development	(Gallego et al., 2001; Barash, 2006)	47	BD	4
ND150	pNFkB	pS529	Mammary gland morphogenesis	(Brantley et al., 2001)	K10-895.12.50	BD	2
EU 151	pEGFR	pY1068	Myoepithelial contractility	(Pasic et al., 2011; Paszek et al., 2005)	Y38	Abcam	2
SM152	pStat1	pY701	Tumor suppressor	(Chan et al., 2012; Haricharan and Li, 2014).	4a	BD	8
EU 153	pAkt	pS473	Survival	(Watson, 2006)	D9E	CST	4
SM 154	pErk1/2	pT202/pY204	Myoepithelial contractility	(Pasic et al., 2011)	20A	BD	4
GD 158	pGsk3	pS9 (Inactivation)	Milk synthesis and cell proliferation	(Dembowy et al., 2015)	D85E12	CST	2
TM169	pPLCgamma2	pY759	Myoepithelial contractility	(Raymond et al., 2011; Reversi et al., 2005)	K86-689.37	BD	1
YB 171	pS6	pS235/pS236	Survival	(Fu et al. 2015; Tumaneng et al. 2012)	N7-548	BD	0.2
GD156	Cyclin B1	Total	Proliferation	(Jin et al., 1998)	GNS-11	BD	2
LU 175	pRb	pS807/811	Proliferation	(Giacinti and Giordano, 2006)	D20B12	CST	0.5
YT 172	Cleaved caspase3	Cleaved@D175	Apoptosis	(Watson, 2006)	5A1E	CST	4

Table S2. Antibody panel (Related to Figure 1). A panel of 29 antibodies is shown, comprising 10 highly informative surface markers, 12 antibody probes against intracellular phosphorylation, 4 antibody probes against the Hippo pathway and 3 antibody probes against cell cycle and apoptosis pathway. Each antibody clone, supplier, epitope and conjugated isotope is indicated. All the antibodies have been previously validated and titrated. References for relevant pathways in the regulation of HMEC are indicated.

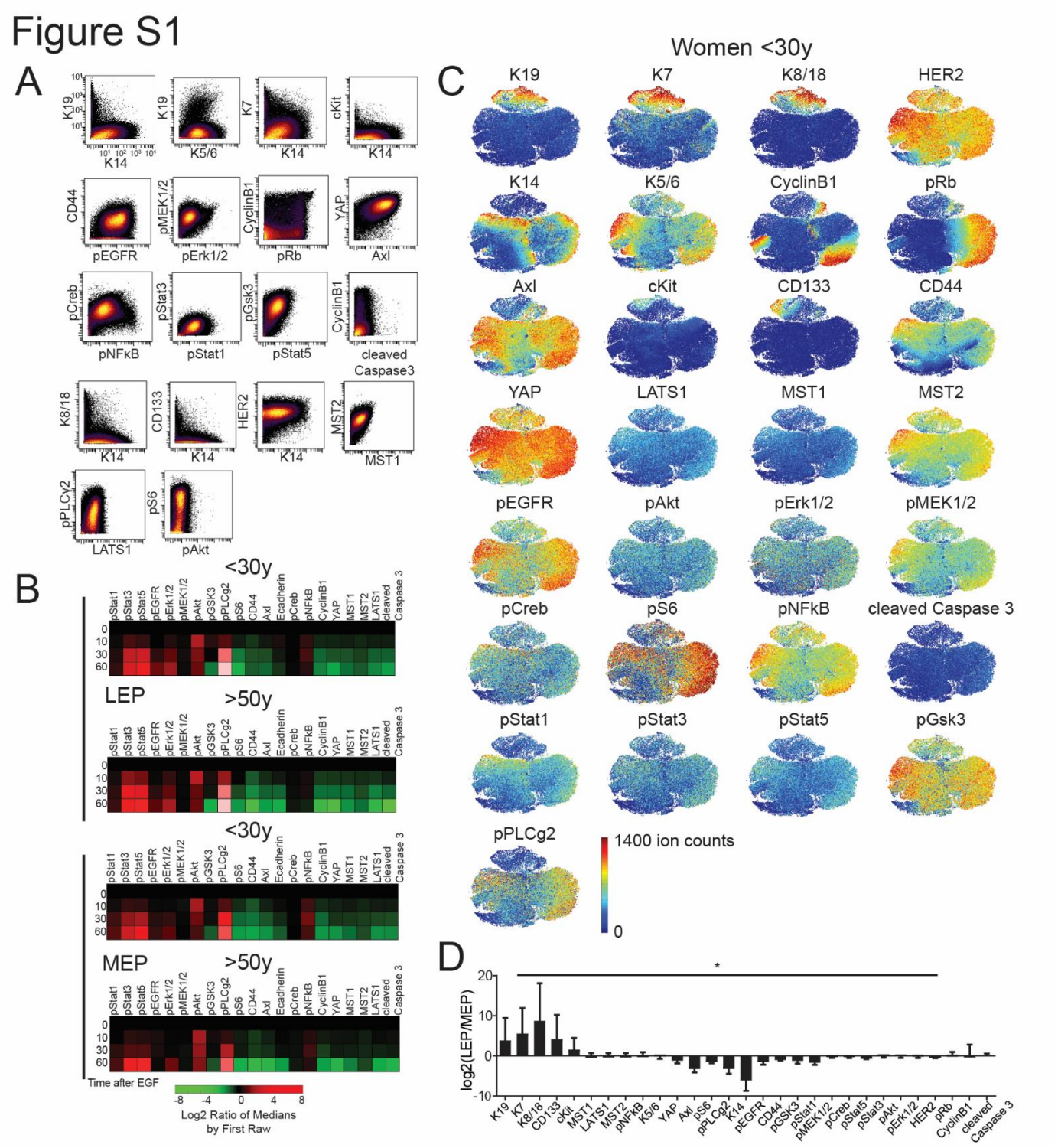

Figure S1. Validation of the antibody panel (Related to Figure 1 and 2). The antibody panel has been extensively validated and titrated (data not shown). The raw data has been transformed with arcsinh with the cofactor of 5. (A) To illustrate the functionality of each metal-conjugated

antibody, representative biaxial plots show staining profiles of the antibodies used in women <30y (merged, N=16), ranging from 10^0 to 10^4 ion counts per cell. (B) Heatmaps of marker expression in HMEC from three <30y and >50y women treated with EGF and vanadate for 60min, manually gated after tSNE projection. At, t=0, 10, 30 and 60min cells were harvested and analyzed with mass cytometry using barcoding and a panel of 23 antibody probes. The fold change of marker expression is ranged from the lowest (green) to the highest (red). This experiment validates the signaling pathway antibodies. (C) tSNE maps from HMEC from women <30y (merged, N=16). Only 50'000 cells are subsampled for display. The marker expression is ranged from 0 (blue) to 1400 ion counts (red). (D) Log_2 fold change in marker expression of LEP over MEP manually gated from tSNE. Paired student t-test was performed on median of protein expression in LEP vs MEP before logarithm transform, * $p<0.05$ N=16.

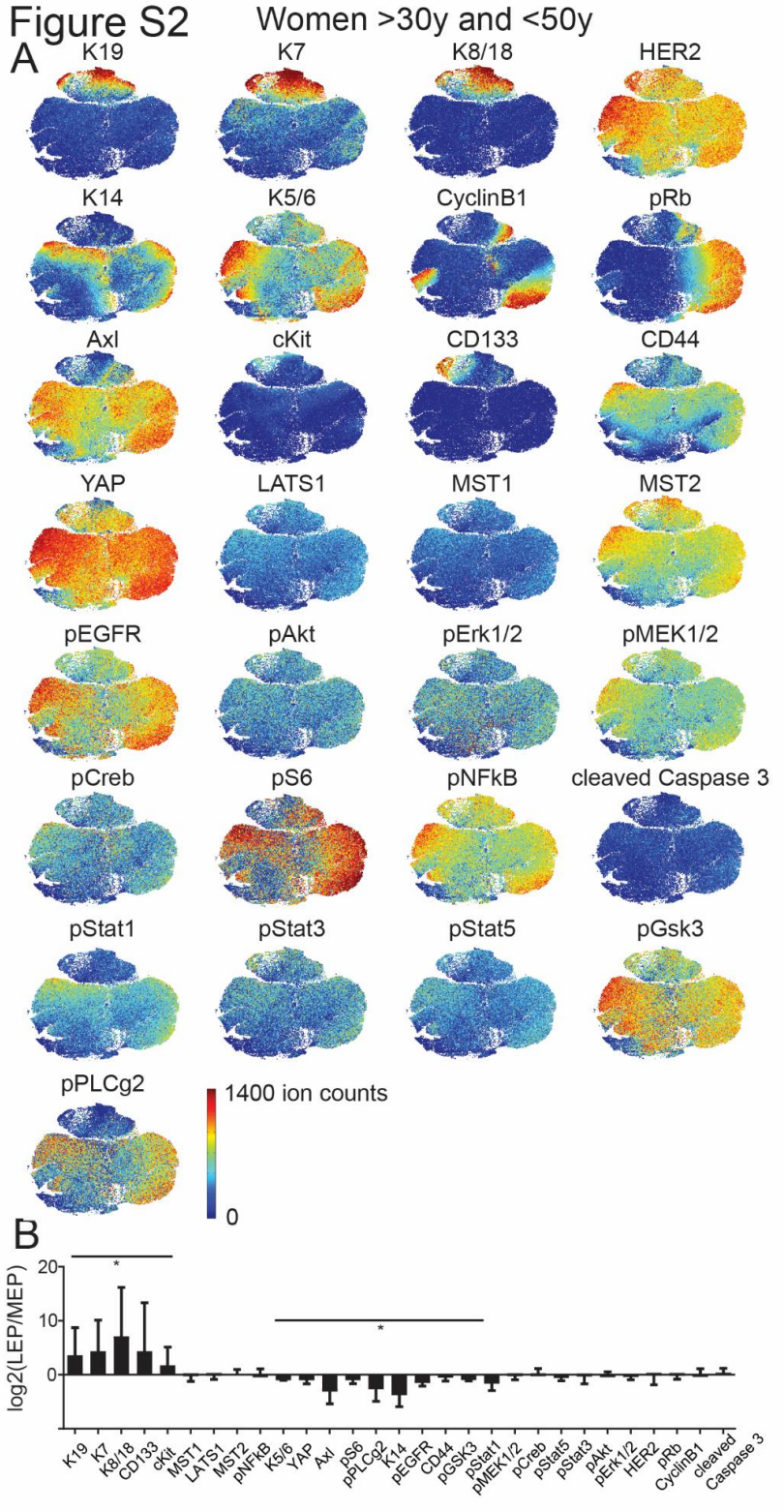

Figure S2. Luminal and myoepithelial lineages exhibit a phenotypic divergence in women >30 and <50y (Related to Figure 2). (A) tSNE maps from HMEC from women >30y and <50y (merged and subsampled at 50'000 cells, N=9). The marker expression is ranged from 0 (blue) to 1400 ion counts (red). (B) Log_2 fold change in marker expression of LEP over MEP manually gated from tSNE. Four abnormal samples were excluded: a sample from milk fluid (250MK), two samples bearing BRCA1 or ATM mutation (90P and 245AT), and one sample from a tumor (173T). Paired student t-test was performed on median of protein expression in LEP vs MEP before logarithm transform. The non-significance was due to a lower sample number (N=9) in addition to age-related changes. Student t-test * $p<0.05$ N=9.

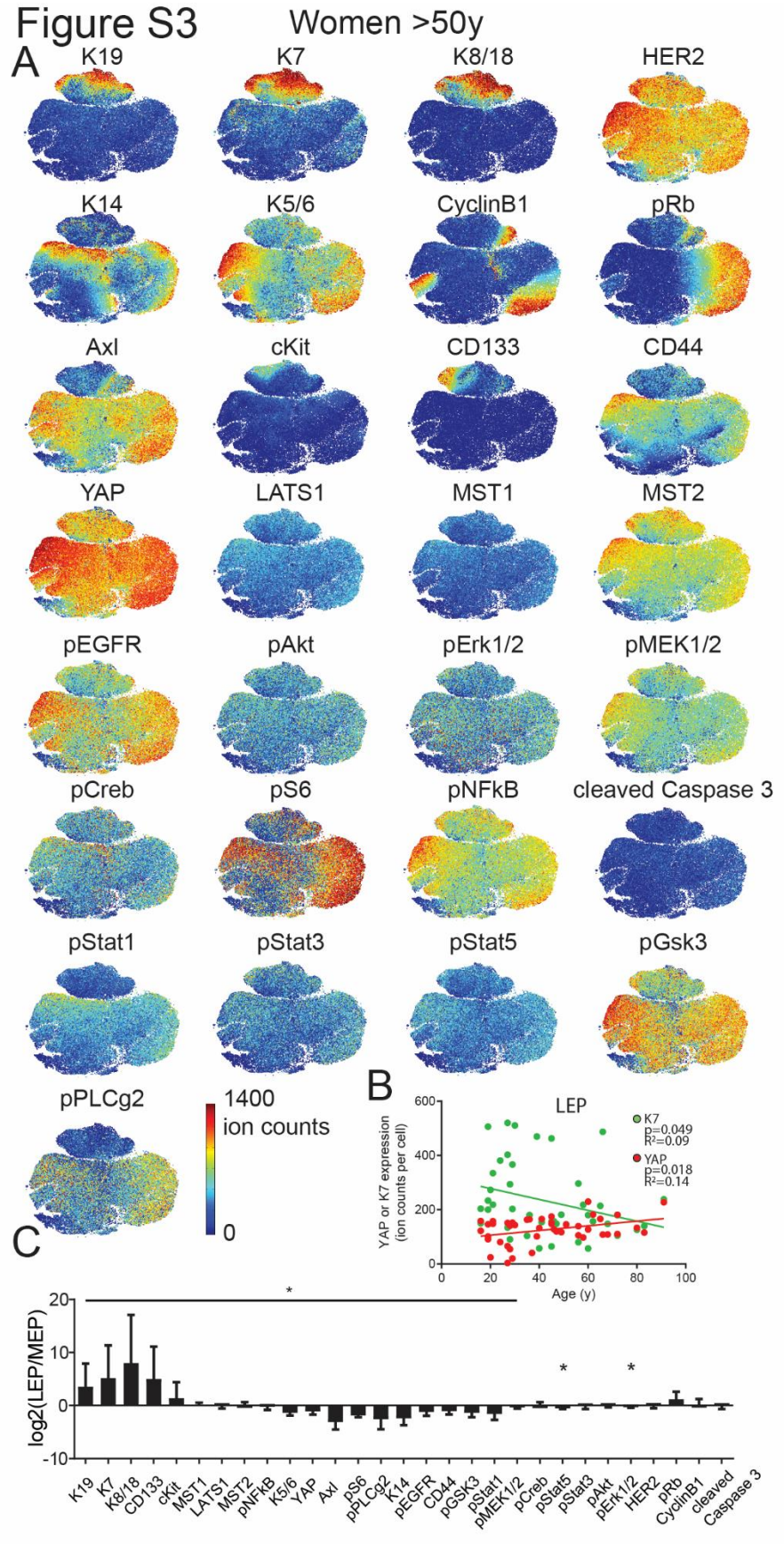

Figure S3. Luminal and myoepithelial lineages exhibit a phenotypic divergence in women >50y (Related to Figure 2). (A) tSNE maps from HMEC from women >50y (merged and subsampled at 50'000 cells, N=15). The marker expression is ranged from 0 (blue) to 1400 ion counts (red). (B) Linear regression of K7 and YAP expression in LEP as a function of age. (C) Log_2 fold change in marker expression of LEP over MEP manually gated from tSNE. Paired student t-test was performed on median of protein expression in LEP vs MEP before logarithm transform, * $p<0.05$ N=15.

Figure S4

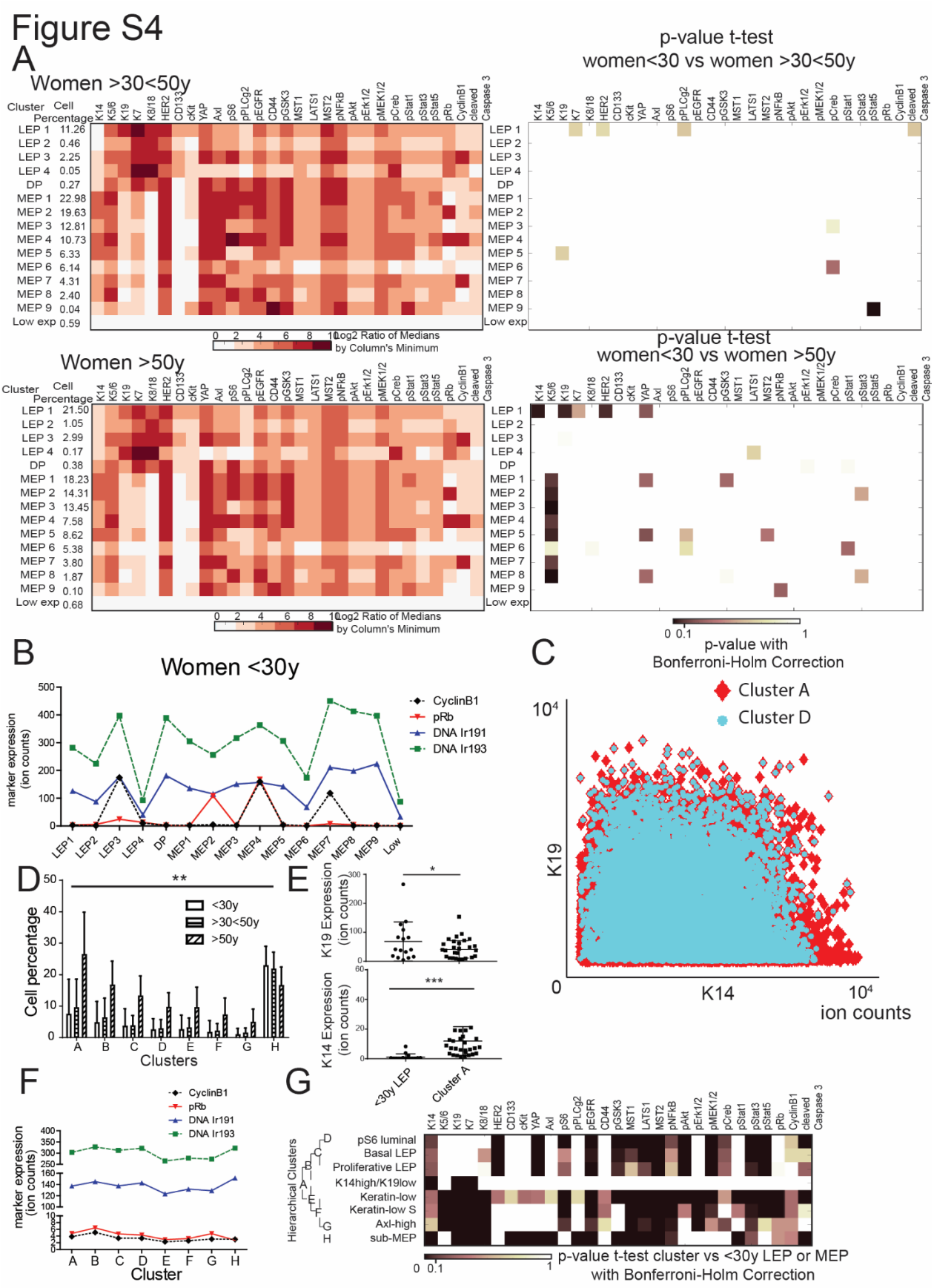
A
Women >30<50y
Women >50y
p-value t-test
women<30 vs women >30<50y
p-value t-test
women<30 vs women >50y
Log2 Ratio of Medians
by Column's Minimum
p-value with
Bonferroni-Holm Correction
B
Women <30y
marker expression
(ion counts)
CyclinB1
pRb
DNA Ir191
DNA Ir193
C
Cluster A
Cluster D
K19
K14
ion counts
D
Cell percentage
<30y
>30<50y
>50y
Clusters
E
K19 Expression
(ion counts)
K14 Expression
(ion counts)
<30y LEP
Cluster A
F
Cluster
G
Hierarchical Clusters
pS6 luminal
Basal LEP
Proliferative LEP
K14high/K19low
Keratin-low
Keratin-low S
Axl-high
sub-MEP
p-value t-test cluster vs <30y LEP or MEP
with Bonferroni-Holm Correction

Figure S4. PhenoGraph analysis identified lineage-specific subsets (Related to Figure 3). (A) Heatmaps of marker expression of each cluster identified with PhenoGraph of HMEC from women >30 and <50y and women >50y with their associated p-values with Bonferroni-Holm correction of student t-tests. (B) Plots show CyclinB1 (black dashed line), pRb (red plain line), Iridium 191 labeling DNA (blue plain line) and Iridium 193 labeling DNA (green dashed line) intensity (ion counts) in each cluster identified with PhenoGraph. LEP3, MEP4 and MEP7 had the highest Cyclin B1 expression which correlated with higher Iridium intensity, thus DNA content, as compared to the other clusters. (C) Scatter plot shows the expression of K14 and K19 in Citrus cluster A (red diamonds) and D (blue dots) to illustrate that cells from cluster D belong to cluster A by hierarchical clustering and thus are superposed onto cells from cluster A. (D) Plots of cell percentage in each Citrus cluster. Four abnormal samples were excluded: 250MK, 90P and 245AT, 173T. (E) Plots show the median expression of K19 and K14 in <30y LEP (n=16) and the cluster A of the Citrus tree (N=40). t-test *** $p<0.0001$, * $p=0.0433$. (F) Plots show CyclinB1 (black dashed line), pRb (red plain line), Iridium 191 labeling DNA (blue plain line) and Iridium 193 labeling DNA (green dashed line) intensity (ion counts) in each cluster identified with Citrus. (G) Heatmaps show the p-values with Bonferroni-Holm correction from student t-tests of each marker expression of Citrus clusters vs LEP or MEP <30y.

Figure S5

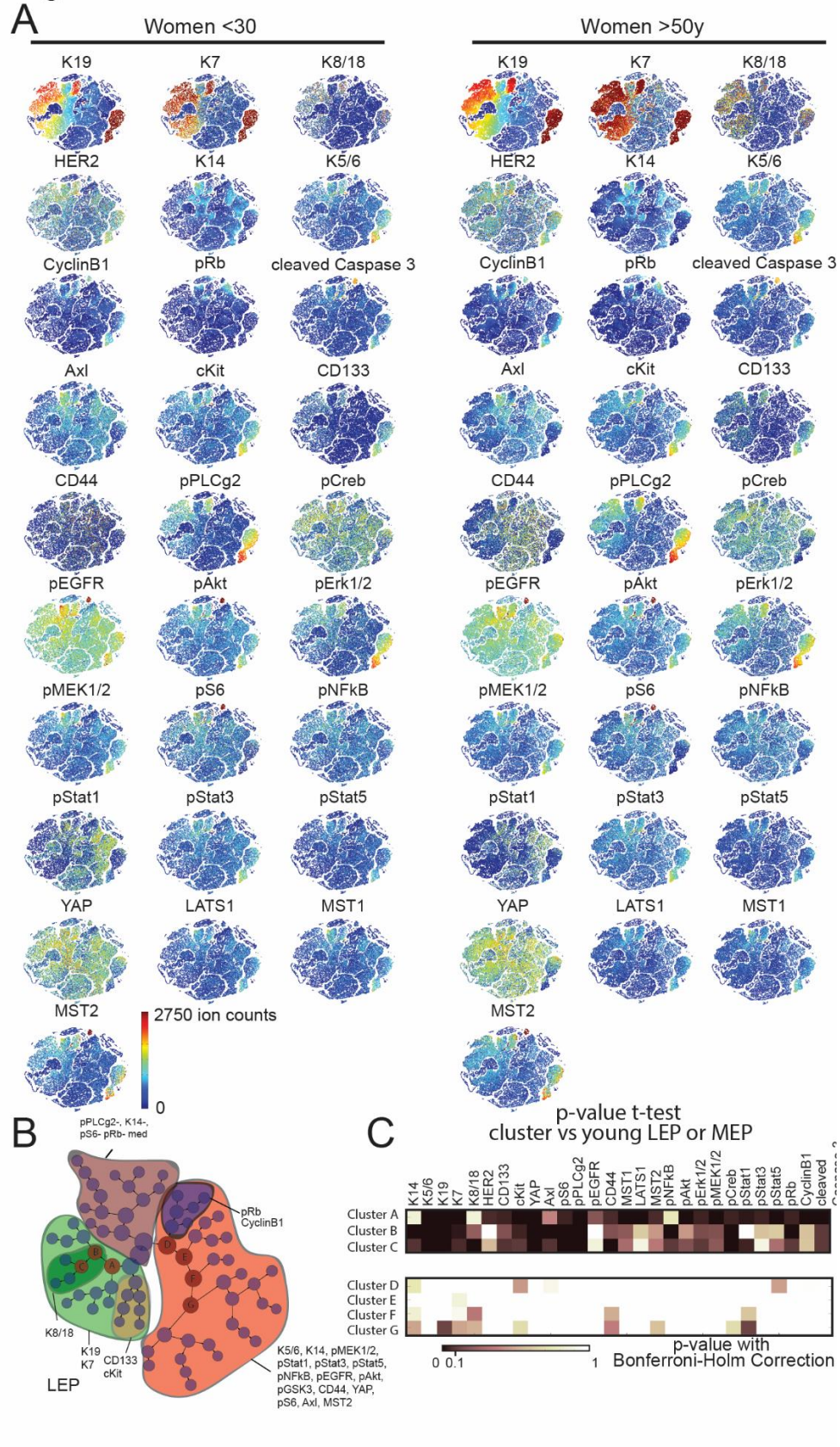
A
Women <30
Women >50y
K19
K7
K8/18
HER2
K14
K5/6
CyclinB1
pRb
cleaved Caspase 3
Axl
cKit
CD133
CD44
pPLCg2
pCreb
pEGFR
pAkt
pErk1/2
pMEK1/2
pS6
pNFkB
pStat1
pStat3
pStat5
YAP
LATS1
MST1
MST2
2750 ion counts
0
B
pPLCg2-, K14-, pS6- pRb- med
pRb CyclinB1
K8/18
K19 K7
CD133 cKit
LEP
K5/6, K14, pMEK1/2, pStat1, pStat3, pStat5, pNFkB, pEGFR, pAkt, pGSK3, CD44, YAP, pS6, Axl, MST2
C
p-value t-test
cluster vs young LEP or MEP
Cluster A
Cluster B
Cluster C
Cluster D
Cluster E
Cluster F
Cluster G
0 0.1
1
p-value with Bonferroni-Holm Correction

Figure S5. High dimensional analysis of cellular heterogeneity within primary human breast epithelia (Related to Figure 5). (A) tSNE maps of breast epithelia from women <30y (merged, and subsampled at 50’000 cells, N=7) and women >50y (merged, and subsampled at 50’000 cells, N=6). The marker expression is ranged from 0 (blue) to 2750 ion counts (red). (B) Hierarchical tree of agglomerative clusters obtained with the Citrus analysis. Node sizes are scaled on the basis of frequency of cells in each cluster. Major cell compartments are contoured on the basis of expression of canonical markers. (C) Heatmaps show the p-values with Bonferroni-Holm correction from student t-tests of each marker expression of Citrus clusters vs LEP or MEP <30y.

Figure S6

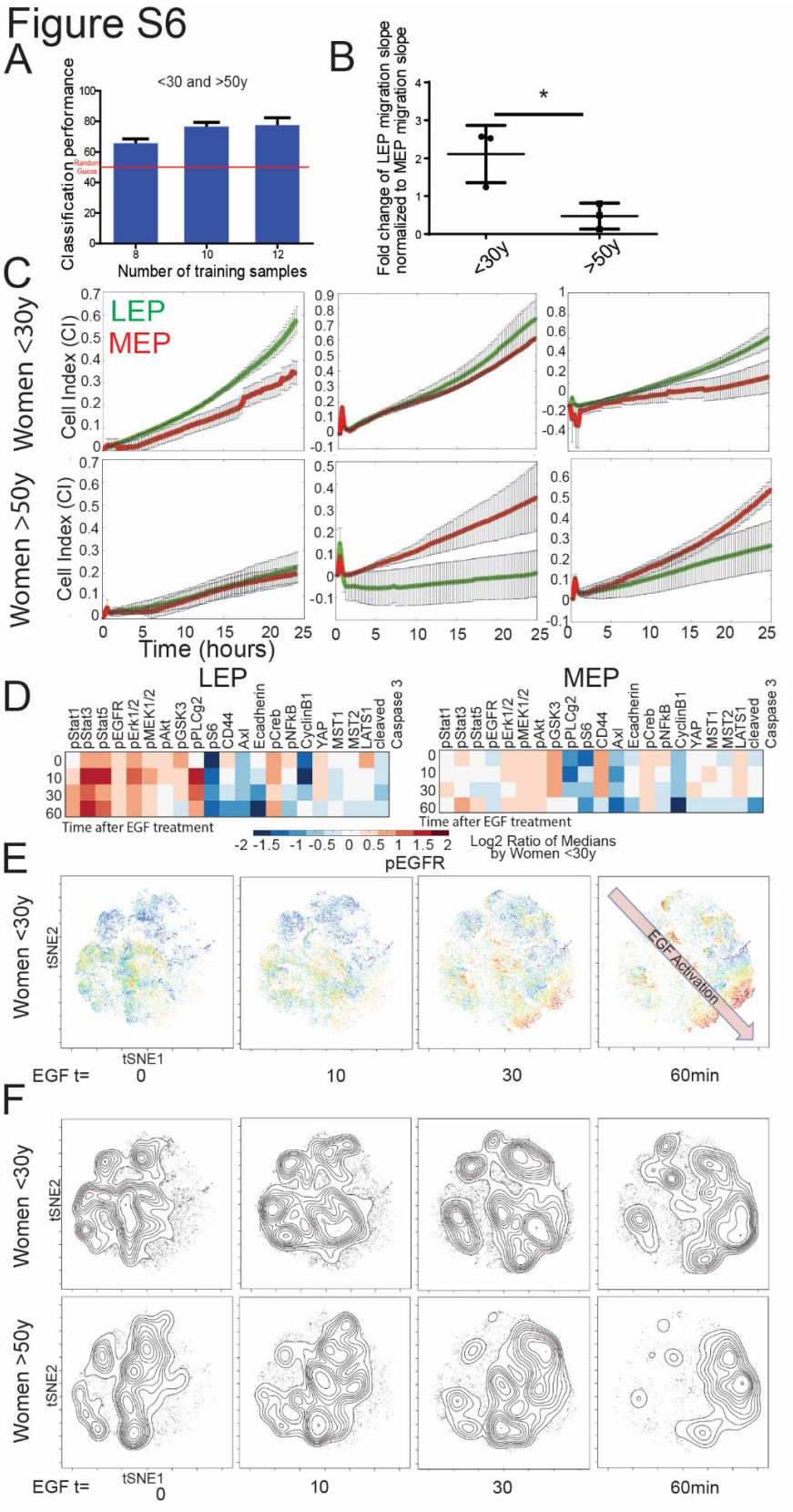
A
<30 and >50y
Classification performance
Random Guess
Number of training samples
B
Fold change of LEP migration slope normalized to MEP migration slope
*
<30y
>50y
C
Women <30y
Women >50y
LEP
MEP
Cell Index (CI)
Time (hours)
D
LEP
MEP
pStat1
pStat3
pStat5
pEGFR
pErk1/2
pMEK1/2
pAkt
pGSK3
pPLCg2
pS6
CD44
Axl
Ecadherin
pCreb
pNFkB
CyclinB1
YAP
MST1
MST2
LATS1
cleaved
Caspase 3
Time after EGF treatment
Log2 Ratio of Medians by Women <30y
pEGFR
E
Women <30y
tSNE2
tSNE1
EGF Activation
EGF t=
0
10
30
60min
F
Women <30y
Women >50y
tSNE2
tSNE1
EGF t=
0
10
30
60min

Figure S6. Evidence of newly acquired functional properties in luminal epithelial cells with age (Related to Figure 6; experimental procedures; data analysis). (A) Citrus classification performance using 8, 10 or 12 training samples. (B) Plots show the fold change of LEP cell migration index (CI) slope normalized to MEP CI migration slope in women <30y and >50y (N=3, p=0.0269). (C) Graphs show CI measured with xCELLigence instrument every 15min for 25h in FACS sorted LEP and MEP from HMEC from three women <30y and from three women >50y. (D) HMEC from three <30y and >50y women were treated with EGF and vanadate for 60min. Heatmaps of marker expression in LEP and MEP manually gated after tSNE projection. Data was normalized to values from <30y women to highlight age-related changes. The $\log_2$ fold change is ranged from the lowest (blue) to the highest (red). (E) tSNE maps of HMEC from women <30y at t=0, 10, 30 and 60min. pEGFR expression from the lowest (blue) to the highest (red) is shown to highlight the movement of HMEC in the phenotypical space upon EGF activation. (F) Density plots in the tSNE phenotypic space exhibited a stronger response in women >50y upon EGF activation. Data are means +/- SEM.

Figure S7

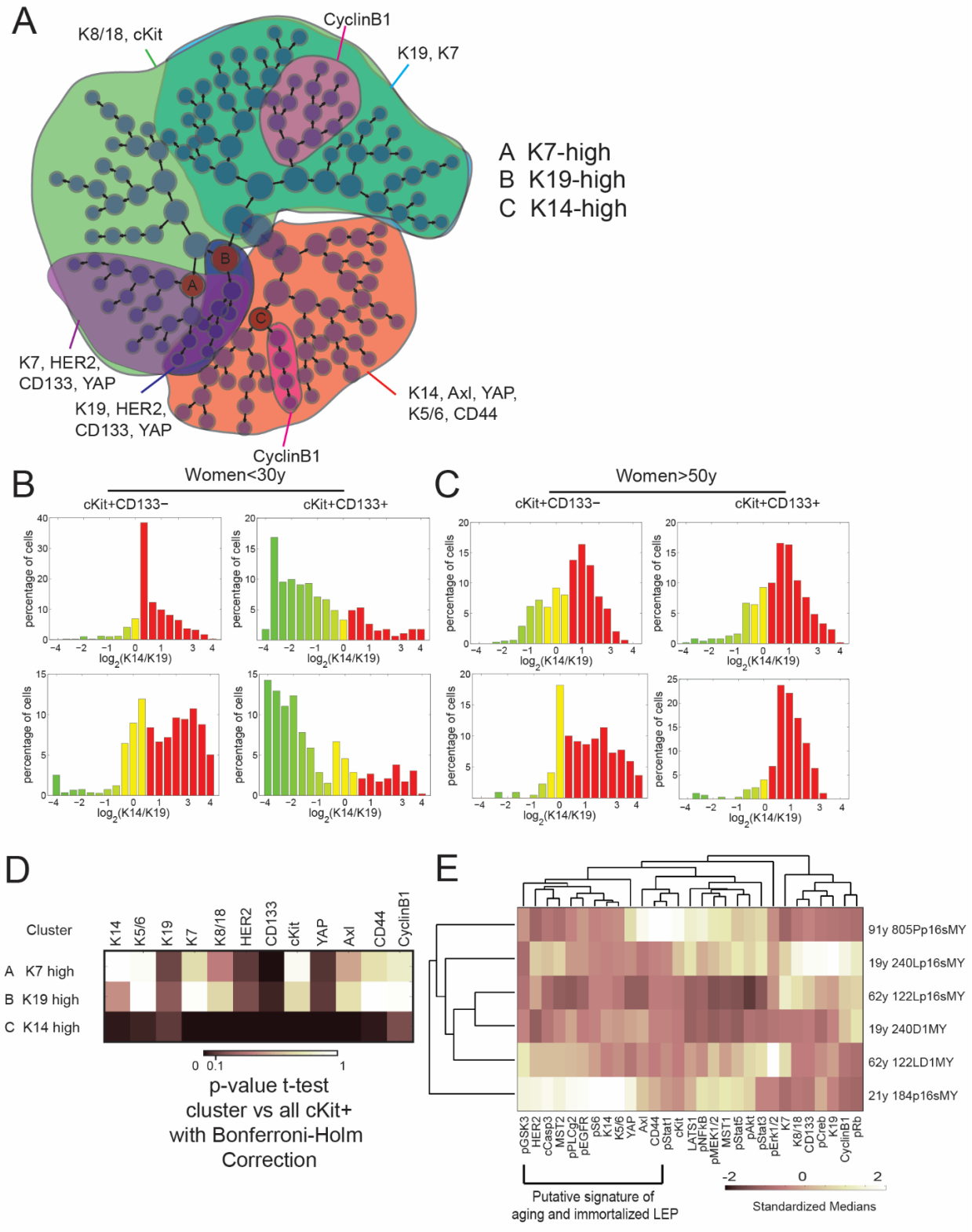
A
K8/18, cKit
CyclinB1
K19, K7
A K7-high
B K19-high
C K14-high
K7, HER2, CD133, YAP
K19, HER2, CD133, YAP
K14, Axl, YAP, K5/6, CD44
CyclinB1
B
Women<30y
cKit+CD133−
cKit+CD133+
C
Women>50y
cKit+CD133−
cKit+CD133+
percentage of cells
log2(K14/K19)
D
Cluster
K14
K5/6
K19
K7
K8/18
HER2
CD133
cKit
YAP
Axl
CD44
CyclinB1
A K7 high
B K19 high
C K14 high
0 0.1 1
p-value t-test cluster vs all cKit+ with Bonferroni-Holm Correction
E
91y 805Pp16sMY
19y 240Lp16sMY
62y 122Lp16sMY
19y 240D1MY
62y 122LD1MY
21y 184p16sMY
pGSK3
HER2
cCasp3
MST2
pPLCg2
pEGFR
pS6
K14
K5/6
YAP
Axl
CD44
pStat1
cKit
LATS1
pNFkB
pMEK1/2
MST1
pStat5
pAkt
pStat3
pErk1/2
K7
K8/18
CD133
pCreb
K19
CyclinB1
pRb
Putative signature of aging and immortalized LEP
-2 0 2
Standardized Medians

Figure S7. Evidence of phenotypic divergence in luminal progenitors with age (Related to Figure 6). (A) Visual representation of unsupervised hierarchical clustering of cKit+ progenitors HMEC with Citrus (N=6). Node sizes are scaled on the basis of frequency of cells in each cluster. Major cell compartments are contoured on the basis of expression of canonical markers. The three clusters changing in abundance with age are shown. (B) Histograms represent log_2-transformed ratios of K14 to K19 protein expression in single cells of acini from two women <30y (124, 29y and 160, 16y) and (C) from two women >50y (335R, 58y and 353P, 72y), histograms are heat-mapped to indicate cells with the phenotypes of K14-/K19+ LEP (green), K14+/K19+ progenitors (yellow), and K14+/K19- MEP (red). (D) Heatmap shows the p-values with Bonferroni-Holm correction from student t-tests of each marker expression of Citrus clusters vs LEP or MEP <30y. (E) Heatmap of marker expression of each immortalized strain, z-score normalized and hierarchically ordered. The fold change of marker expression is ranged from the lowest (black) to the highest (white).

Supplemental Experimental Procedures

Generation of immortal cell lines – Finite lifespan HMEC from specimens 184, 240L, 122L, and 805P were obtained from reduction mammoplasty tissues or peripheral to mastectomy tissues (i.e. 805P). HMEC were grown in M87A supplemented with CT at 0.5 ng/ml, and X (Bachem) at 0.1 nM. Retroviral vectors: The p16 shRNA was in the MSCV vector, c-Myc wsa in the pBabe–hygro (BH2) or LXSN vector. Retroviral stocks were generated from supernatants collected in M87A medium. Strains 240L, 122L, and 805P at passage 3 or and 184 at passage 4 were transduced with MSCV-p16sh or MSCV control and selected with puromycin. At the next passage, after puromycin selection, the p16sh transduced cells were transduced with c-Myc pBabe–hygro (c-myc LXSN for 184) and selected with hygromycin. Vector only control pre-stasis cells entered stasis at passage 12-15, whereas the immortalized lines continued to grow.

Mass cytometry analysis. The age of the strains were not known at the time of the experiment. Cells were analyzed on a CyTOF mass cytometer (DVS Sciences) at an event rate of ~500 cells per second. The settings of the instrument and the initial post-processing parameters were described previously. For each barcoded sample several data files were recorded. The files were concatenated using the Cytobank concatenation tool, normalized and debarcoded.

Flow Cytometry – HMEC at fourth passage were trypsinized and resuspended in their media. For enrichment of progenitor, luminal or myoepithelial lineages, anti -CD133-PE-Vio615 (Myltenyi clone AC133, 1:50) anti -CD117-PE (BioLegend, clone 104D2, 1:200), or anti-CD227-FITC (BD; cloneHMPV;1:50), anti-CD10-phycoerythrin (BioLegend; clone HI10a; 1:100), respectively, were added to the media for 25 minutes on ice, washed in PBS, and sorted using FACS Vantage DIVA (Becton Dickinson).

Matrigel/collagen assay – 24-well plates were coated with 50µL of Matrigel as a bottom layer. To create the matrigel/collagen mixture, 50'000 cells in 70µL of media were mixed with 15µL of neutralization solution (100mM Hepes, pH 7.3 in 2X PBS), and 15µL of collagen solution (Corning 354249, 8.69mg/mL), and 100µL of Matrigel for a final concentration of 0.67mg/mL of collagen I. After 3 weeks, gel smears were fixed in methanol:acetone.

Immunofluorescence – Matrigel smears were fixed in methanol:acetone (1:1) at -20°C for 20 minutes, blocked with PBS, 5% normal goat serum, 0.1% Triton X-100, and incubated with anti-K14 (1:1000, Covance, polyclonal) and anti-K19 (1:10, Developmental Studies Hybridoma Bank, clone Troma-III) overnight at 4°C, then visualized with fluorescent secondary antibodies (Invitrogen) incubated with sections for 2 hours at room temperature. EdU was added to culture media 4h prior to fixing cells, and was imaged with A647 click reagents (Invitrogen). Cells were imaged with LSM510 confocal microscope (Carl Zeiss). Image analyses were conducted using a modified watershed method in Matlab software (Mathworks).

Immunostaining of tissue sections- Healthy breast tissue sections were obtained through University of California Davis in accordance with all IRB procedures. Paraffin-embedded sections were deparaffinized and antigen retrieved (Vector Laboratories) and stained with primary antibodies to K14 (1:1'000; Covance; PRB-155P; visualized with A647 Zenon probes from Invitrogen), and K19 (1:100; Abcam; AAH07628). Cells were imaged with LSM710 confocal microscope (Carl Zeiss).

Classification using morphometric context- Each image was represented as its Cellular Morphometric Context, which was constructed as the histogram of cellular morphometric subtypes derived from the cellular morphometric features (K14/K19 signals) through K-Means (dictionary size =1024). Homogeneous kernel map was then applied on the Cellular Morphometric Context representation, so that linear support vector machine (SVM) could be adopted for efficient and effective differentiation among age groups.

xCELLigence analysis- The lower xCELLigence chambers were filled with M87A media with 10% FBS and the upper chamber were filled with $4x10^5$ cells in serum-free M87 media. Cell Index (CI) and slopes were measured using the RTCA-DP instrument.

R code for Citrus classification-

```
library("citrus")
# Where the data lives
dataDirectory = "C:/Users/Fanny/Documents/Cytof/The ladies/"

# List of files to be clustered= your training set
fileList1 = data.frame(c("30_Ladies01_B10_123.fcs","20_Ladies01_E10_160.fcs", "30_Ladies01_C5_195L.fcs", "30_Ladies01_B7_184.fcs", "60_Ladies01_C3_191L.fcs", "70_Ladies01_F4_29.fcs", "70_Ladies01_E8_122L.fcs","80_Ladies01_F5_429ER.fcs"))

# List of files to be mapped= your entire test set
fileList2 = data.frame(c("20_Ladies01_B11_407P.fcs", "20_Ladies01_C9_399E.fcs", "20_Ladies01_E10_160.fcs", … include all files… "100_Ladies01_B2_805P.fcs")

# Read the data
citrus.combinedFCSSet1 = citrus.readFCSSet(dataDirectory,fileList1,fileSampleSize = 5000)
citrus.combinedFCSSet2 = citrus.readFCSSet(dataDirectory,fileList2,fileSampleSize = 5000)

# List of columns to be used for clustering
clusteringColumns = c(surface markers)

# Cluster first dataset
citrus.clustering = citrus.cluster( citrus.combinedFCSSet1, clusteringColumns, minimumClusterSizePercent = 0.1)

# Map new data to exsting clustering
```

```
citrus.mapping = citrus.mapToClusterSpace(citrus.combinedFCSSet.new = citrus.combinedFCSSet2, citrus.combinedFCSSet.old = citrus.combinedFCSSet1, citrus.clustering)

# Large Enough Clusters
largeEnoughClusters = citrus.selectClusters(citrus.clustering)

# Clustered Features and mapped features
clusteredFeatures = citrus.calculateFeatures(citrus.combinedFCSSet1, clusterAssignments = citrus.clustering$clusterMembership, clusterIds = largeEnoughClusters)
mappedFeatures = citrus.calculateFeatures(citrus.combinedFCSSet2 ,clusterAssignments = citrus.mapping$clusterMembership, clusterIds= largeEnoughClusters)

# Labels
# Labels for training set
labels = as.factor(c("Young","Young","Young","Young","Old","Old","Old","Old"))
trainingLabels = as.factor(c("Young","Young","Young","Young","Old","Old","Old","Old"))
#Labels for test set
testingLabels  = as.factor(c(rep("<30",16),rep(">30<50",13),rep(">50",15)))



# Build Endpoint Model
citrus.endpointModel = citrus.buildEndpointModel(clusteredFeatures, trainingLabels)

# Calculate regularization thresholds
regularizationThresholds = citrus.generateRegularizationThresholds( features= clusteredFeatures, labels=trainingLabels, modelType="pamr",family="classification")

# Calculate CV Error rates
thresholdCVRates = citrus.thresholdCVs.quick( modelType="pamr", features=clusteredFeatures, labels=trainingLabels, regularizationThresholds,family="classification")
```

```
# Get pre-selected CV Minima
cvMinima = citrus.getCVMinima("pamr",thresholdCVRates)

# Predict lables of testing data at CV.1se
predictions = citrus.predict( citrus.endpointModel, newFeatures=mappedFeatures)
[,cvMinima$cv.1se.index]

# Contingency Table of results
table(predictions,testingLabels)
```